Redox Biology 63 (2023) 102741

Contents lists available at ScienceDirect

Redox Biology

journal homepage: www.elsevier.com/locate/redox

Hypothalamic JNK1-hepatic fatty acid synthase axis mediates a metabolic rewiring that prevents hepatic steatosis in male mice treated with olanzapine via intraperitoneal: Additional effects of PTP1B inhibition

Vitor Ferreira [a,b], Cintia Folgueira [c], María García-Altares [b,d], Maria Guillén [a,1], Mónica Ruíz-Rosario [e,1], Giada DiNunzio [f,1], Irma Garcia-Martinez [a,b], Rosa Alen [a,b], Christoph Bookmeyer [d], John G. Jones [f], Juan C. Cigudosa [e], Pilar López-Larrubia [a], Xavier Correig-Blanchar [b,d,g], Roger J. Davis [h], Guadalupe Sabio [c], Patricia Rada [a,b,**], Ángela M. Valverde [a,b,*]

[a] Instituto de Investigaciones Biomedicas Alberto Sols (IIBM), CSIC-UAM, Madrid, Spain
[b] CIBER de Diabetes y Enfermedades Metabólicas Asociadas (CIBERDEM), ISCIII, Spain
[c] Centro Nacional de Investigaciones Cardiovasculares (CNIC), 28029, Madrid, Spain
[d] Rovira I Virgili University, Department of Electronic Engineering, Tarragona, Spain
[e] NIMGenetics, Madrid, Spain
[f] Center for Neurosciences and Cell Biology, University of Coimbra, UC-Biotech, Biocant Park, Cantanhede, Portugal
[g] Institut D'Investigacio Sanitària Pere Virgili (IISPV), Tarragona, Spain
[h] Program in Molecular Medicine, Chan Medical School, University of Massachusetts, Worcester, USA

ARTICLE INFO

Keywords:
Olanzapine
Hypothalamus
Inter-organ crosstalk
Metabolic side-effects
Liver
PTP1B

ABSTRACT

Olanzapine (OLA), a widely used second-generation antipsychotic (SGA), causes weight gain and metabolic alterations when administered orally to patients. Recently, we demonstrated that, contrarily to the oral treatment which induces weight gain, OLA administered via intraperitoneal (i.p.) in male mice resulted in body weight loss. This protection was due to an increase in energy expenditure (EE) through a mechanism involving the modulation of hypothalamic AMPK activation by higher OLA levels reaching this brain region compared to those of the oral treatment. Since clinical studies have shown hepatic steatosis upon chronic treatment with OLA, herein we further investigated the role of the hypothalamus-liver interactome upon OLA administration in wild-type (WT) and protein tyrosine phosphatase 1B knockout (PTP1B–KO) mice, a preclinical model protected against metabolic syndrome. WT and PTP1B–KO male mice were fed an OLA-supplemented diet or treated via i.p. Mechanistically, we found that OLA i.p. treatment induces mild oxidative stress and inflammation in the hypothalamus in a JNK1-independent and dependent manner, respectively, without features of cell dead. Hypothalamic JNK activation up-regulated lipogenic gene expression in the liver though the vagus nerve. This effect concurred with an unexpected metabolic rewiring in the liver in which ATP depletion resulted in increased AMPK/ACC phosphorylation. This starvation-like signature prevented steatosis. By contrast, intrahepatic lipid accumulation was observed in WT mice treated orally with OLA; this effect being absent in PTP1B–KO mice. We also demonstrated an additional benefit of PTP1B inhibition against hypothalamic JNK activation, oxidative stress and inflammation induced by chronic OLA i.p. treatment, thereby preventing hepatic lipogenesis. The protection conferred by PTP1B deficiency against hepatic steatosis in the oral OLA treatment or against oxidative stress and neuroinflammation in the i.p. treatment strongly suggests that targeting PTP1B might be also a therapeutic strategy to prevent metabolic comorbidities in patients under OLA treatment in a personalized manner.

* Corresponding author. Instituto de Investigaciones Biomedicas Alberto Sols (IIBM), CSIC-UAM, Madrid, Spain.
** Corresponding author. Instituto de Investigaciones Biomedicas Alberto Sols (IIBM), CSIC-UAM, Madrid, Spain.
E-mail addresses: prada@iib.uam.es (P. Rada), avalverde@iib.uam.es (Á.M. Valverde).
[1] These authors contributed equally in this manuscript.

https://doi.org/10.1016/j.redox.2023.102741
Received 21 April 2023; Received in revised form 9 May 2023; Accepted 10 May 2023
Available online 15 May 2023
2213-2317/© 2023 The Authors. Published by Elsevier B.V. This is an open access article under the CC BY-NC-ND license (http://creativecommons.org/licenses/by-nc-nd/4.0/).

Abbreviations

SGAs	second generation antipsychotic
OLA	olanzapine
NAFLD	non-alcoholic fatty liver disease
PCSK9	Proprotein subtilisin kexin type 9
CNS	central nervous system
JNK	c-Jun N-terminal Kinase
NPY	neuropeptide-Y
AgRP	agouti-related peptide
MIF	migration inhibitory factor
AMPK	AMP-activated protein kinase
ROS	reactive oxygen species
PTP1B	protein tyrosine phosphatase 1B
T2D	type 2 diabetes
p38-MAPK	p38-mitogen-activated protein kinase
ER	endoplasmic reticulum
i.p.	intraperitoneal
BAT	brown adipose tissue
WT	wild-type
ACC	acetyl CoA carboxylase
KO	knockout
VEH	vehicle
VMH	ventromedial nucleus of the hypothalamus
AAV	adeno-associated viruses
EDTA	ethylenediamine tetraacetic acid
LC-MS/MS	liquid chromatography-tandem mass spectrometry
MRI	magnetic resonance imaging
TG	triglyceride
^{2}H-NMR	^{2}H nuclear magnetic resonance
MTBE	methyl-tert-butyl ether
f.i.d.	free-induction decays
PFA	paraformaldehyde
FBS	fetal bovine serum
NAC	N-acetylcysteine
iPTP1B	PTP1B pharmacological inhibitor
BSA	bovine serum albumin
SDS-PAGE	SDS-polyacrylamide gel electrophoresis
PCA	principal component analysis
DEGs	differentially expressed genes
DAPI	4,6-diamidino-2-phenylindole
EB	equilibration buffer
TMS	tetramethylsilane
LDI–MS	laser desorption/ionization–mass spectrometry
FA	fatty acid
PC	phosphatidylcholine;
SM	sphingomyelin
PE	phosphatidylethanolamine
PUFA	polyunsaturated fatty acids
DHA	docosahexaenoic acid
ARA	arachidonic acid plus
EPA	eicosapentaenoic acid
GFAP	glial fibrillary acidic protein
Iba1	ionized calcium-binding adapter molecule 1

1. Introduction

Schizophrenia is a severe chronic psychiatric disorder that affects about 24 million people worldwide. According to current clinical guidelines, second generation antipsychotics (SGAs) are the first line of life-long chronic treatment for schizophrenia [1,2]. However, in a high proportion of patients on SGA treatment severe metabolic dysfunctions such as abnormal body weight gain, hyperglycemia and dyslipidemia have been reported [3–5]. This association between metabolic complications and SGAs was evidenced in a meta-analysis review of several clinical trials in healthy volunteers showing the ability of these drugs to directly and independently favor weight gain and insulin resistance [6]. Furthermore, another analysis of randomized trials from 1955 to 2012 concluded that the SGAs with higher risk of weight gain were olanzapine (OLA) [7], highly used in the clinic [8,9], zotepine and clozapine [7].

Overweight and obesity are major risk factors for non-alcoholic fatty liver disease (NAFLD), a worldwide epidemic with an exponential growth also associated with insulin resistance and inflammation [10–12]. Notably, the incidence of NAFLD is increased in patients with mental illness [13], being even higher in patients under treatment with SGAs [14]. Importantly, as previously reviewed [15], different drivers of oxidative stress contribute to NAFLD progression by inducing or boosting inflammation. Oxidative stress is also directly related with the presence of several reactive metabolites that favor lipotoxic liver injury and the evolution to more severe NAFLD stages.

OLA has been shown to induce, directly or through extrahepatic effects, lipid accumulation in the liver. In this regard, male rats treated with OLA via gastric tube presented liver steatosis [16]. Moreover, female mice treated daily with OLA via oral gavage displayed intrahepatic lipid accumulation independent of body weight changes in parallel to an increase in hepatic proprotein subtilisin kexin type 9 (PCSK9) [17] or sortilin expression [18]. Additionally, signals emerging from the central nervous system (CNS) have been shown to drive abnormalities in peripheral lipid metabolism. In this line, central triiodothyronine (T_3) administration activates hypothalamic c-Jun N-terminal Kinase (JNK) that favors hepatic lipogenesis [19]. Related with OLA, female rats treated via intragastric administration showed lipid disturbances associated with weight gain and dyslipidemia that paralleled with an up-regulation of the appetite-related neuropeptide-Y/agouti-related peptide (NPY/AgRP) in the hypothalamus [20]. These effects were associated with a reduction in the abundance of short-chain fatty acids (FA) and 5-hydroxytryptamine (serotonin) levels in rat cecum. Furthermore, the abnormal lipid metabolism caused by OLA treatment was associated to the vagus nerve-mediated gut microbiota-brain axis [20]. On the other hand, OLA-mediated effects have been also reported in the immune system. Cui and coworkers found that plasma levels of macrophage migration inhibitory factor (MIF) were increased in individuals under OLA treatment. Importantly, MIF was elevated in the hypothalamus of female mice receiving an OLA oral treatment concomitantly to hyperphagia due to the activation of appetite-related AMP-activated protein kinase (AMPK) and AgRP-related signaling pathways [21]. The relevance of hypothalamic MIF was evidenced by the protection against OLA-induced glucose and lipid metabolic disturbances in global MIF-deficient mice or upon central injection of a neutralizing anti-MIF antibody prior to OLA treatment [21]. Moreover, a clinical study with 14 drug-naive patients with first psychotic episode has shown that IL-27 and IL-6 plasma levels may be biomarkers for the efficacy of OLA treatment [22], supporting its immunomodulatory effects. However, the association between OLA and the induction of reactive oxygen species (ROS) production is yet poorly understood. Whereas OLA increased ROS levels in whole blood of rats [23] and potentiated general oxidative stress hallmarks in mHypoA-59 hypothalamic neurons in culture [24], it has been shown to have some antioxidant properties in cultured neutrophils [25]. Therefore, additional studies are needed to evaluate the contribution of oxidative stress and inflammation to OLA-mediated metabolic side-effects.

Protein tyrosine phosphatase 1B (PTP1B) is a negative regulator of leptin and insulin signaling and is currently considered a therapeutic target for obesity and type 2 diabetes (T2D) due to the results of many preclinical studies conducted in global or tissue-specific mice deficient

in the *Ptpn1* gene encoding PTP1B [26–29]. Regarding oxidative stress, PTP1B deficiency protected hepatocytes against paracetamol-induced cell death by preventing glutathione reduction, generation of ROS and the activation of JNK and p38-mitogen-activated protein kinase (p38-MAPK) [30]. Notably, its inhibition in HepG2 cells prevents apoptosis induced by palmitate and oleate by improving mitochondrial dynamics and reducing oxidative and endoplasmic reticulum (ER) stress [31].

Very recently, we reported a potential therapeutic advantage of OLA intraperitoneal (i.p.) compared to oral administration in preventing weight gain in male mice. This beneficial effect was associated with higher OLA levels in plasma and hypothalamus that controlled an AMPK-driven hypothalamus-brown adipose tissue (BAT) axis, preventing weight gain in a PTP1B-independent manner [32]. Importantly, PTP1B deficiency protected against weight gain associated with the dietary OLA treatment by increasing energy expenditure (EE). These previous results prompted us to investigate in more depth the intra- and extra-hypothalamic effects elicited by the higher OLA levels reaching the hypothalamus upon its administration via i.p. In particular, we focused in the hypothalamus-liver axis that, in response to other stimuli such as T_3 [19], oleic acid [33] or corticotropin-releasing factor [34], modulates lipid metabolism [19]. As expected, wild-type (WT) mice fed an OLA-supplemented diet presented, concomitantly to hyperphagia and weight gain, intrahepatic lipid accumulation, whereas PTP1B-deficient mice were protected against OLA-induced hepatic steatosis. Unexpectedly, even though WT mice under the OLA i.p. treatment lost weight, fatty acid synthase (FAS) protein levels, as well as its transcriptional regulatory cascade, were upregulated in the liver, an effect controlled by hypothalamic JNK1 activation induced by higher OLA levels reached in this brain region during the i.p. treatment. This molecular signature paralleled with oxidative stress and inflammation in the hypothalamus. Interestingly, hypothalamic-mediated FAS upregulation by OLA i.p. treatment did not result in steatosis due to a metabolic rewiring involving hepatic ATP levels, AMPK and acetyl CoA carboxylase (ACC). Remarkably, hypothalamic JNK activation, oxidative stress and neuroinflammation were absent in PTP1B–KO mice.

2. Material and methods

Antibodies for Western blot and immunohistochemistry/immunofluorescence and primers used for qRT-PCR are listed in Supplementary Tables 1, 2 and 3 respectively.

2.1. Animals and treatments

Three-months-old WT and PTP1B-knockout (KO) male mice on the C57BL/6J × 129 Sv/J genetic background [35] and age-matched C57BL/6J and JNK2-KO/JNK1$^{flox\text{-}flox}$ male mice were used. Animal studies were approved by the Ethics Committee of Consejo Superior de Investigaciones Científica (CSIC, Spain) and conducted in accordance with the guidelines for animal care of Comunidad de Madrid and Directive 2010/63/EU. Animals were maintained at 22–24 °C and 55% humidity on 12 h light/dark cycles (starting at 8 a.m.) and fed a regular rodent chow diet (A04, Panlab, Barcelona, Spain) and tap water *ad libitum*.

OLA-supplemented diet treatment: WT and PTP1B–KO mice were fed a chow diet supplemented or not with OLA (GP8311, Glentham Life Sciences, Corsham, UK) for 7 months. OLA dosage in the diet was calculated taking into account an average mice weight of 30–35 g and average food intake of 4 g/day, corresponding to 5 mg/kg/day. This dose was chosen based on previous studies in rodents treated orally with OLA at 5–10 mg/kg/day including a recent study by our group [32] showing hyperphagia and weight gain [36–39] and resulting in steady-state plasma levels of the drug close to the therapeutic range [39]. Since mice treated with OLA supplemented in the diet presented hyperphagia as we previously reported [32], mice received approximately 10 mg/kg OLA.

OLA intraperitoneal (i.p.) treatment: Mice received vehicle (VEH) (2% v/v DMSO in 0.9% NaCl) or 10 mg/kg/day OLA via i.p. injection (10–12 a.m.) for 8 weeks as reported for injectable treatments [40–44], including a recent study by our group [32]. This OLA dosage was equivalent to that received orally via supplemented diet. Another cohort of mice was treated with OLA at 5 mg/kg/day.

OLA treatment by oral gavage: mice received a daily (10–12 a.m.) oral gavage of OLA at 10 mg/kg, dose previously reported for oral treatment by our group and others [32,37,39,45–48], or VEH (4% v/v DMSO in 0.9% NaCl) for 8 weeks.

OLA intrahypothalamic injections: during the light phase of the diurnal cycle (8 a.m.-1 pm), mice were anesthetized with isoflurane for ~5 min prior to the intrahypothalamic injection and placed in the stereotaxic apparatus. Then, mice received bilaterally a single injection of OLA (15 nmol, dose used in previous studies [32,49]) or DMSO in the ventromedial nucleus of the hypothalamus (VMH) at the coordinates 1.46 mm posterior, ±0.5 mm lateral and 5.5 mm depth to Bregma [50]. During the injection, mice remained anesthetized with isoflurane. To minimize backflow up the needle track, the needle remained inserted for approximately 3–5 min after injection. In order to generate mice lacking JNK1 and JNK2 in the hypothalamus, C57BL/6J JNK2-KO/JNK1$^{flox\text{-}flox}$ mice were injected adeno-associated viruses encoding Cre recombinase (AAV-Cre, SignaGen Laboratories, Rockville, MD, USA) in the VMH using the aforementioned coordinates (1 μl/injection site), as previously reported [19,32,51,52] prior to OLA i.p. treatment for 8 weeks with OLA (10 mg/kg/day) as described above. In parallel, JNK2-KO/JNK1$^{flox\text{-}flox}$ mice were injected AAV-GFP (Viraquest Inc., North Liberty, IA, USA) as controls. In another experiments, C57BL/6J male mice were injected adenoviruses encoding for AMPKα1-CA (Viraquest) in the VMH (1 μl/injection site), as previously reported by our group [32] and others [19,51,52], five days before the OLA central injection (15 nmol, 30 min).

2.2. Measurement of OLA levels in plasma and hypothalamus

As we described previously [32], mice received a single i.p. injection or a single oral gavage of OLA at the dose of 10 mg/kg. Two hours after administration, animals were anesthetized with isoflurane and blood was collected via intracardiac puncture with ethylenediamine tetraacetic acid (EDTA). The brain was removed from the skull and the hypothalamus was collected. Blood was immediately centrifuged at 15 600 g for 20 min at 4 °C and plasma samples were stored at −80 °C. The hypothalami were homogenized in ice-cold 1.89% (v/v) formic acid in water, centrifuged at 15 600 g for 20 min at 4 °C and the supernatants were stored at −80 °C (adapted from Wojnicz et al. [53]). A simple and sensitive liquid chromatography-tandem mass spectrometry (LC-MS/MS, Agilent Technologies, Spain) method was used for the determination of OLA, as reported previously [32,54]. OLA and their isotope-labeled internal standards were extracted from 100 μl of plasma by protein precipitation. A combination of formic acid (0.2%)-acetonitrile (pH 3.0; 65:35, v/v) was used as mobile phase and the chromatogram was run under gradient conditions at a flow rate of 0.6 ml/min. Run time lasted 6 min, followed by a re-equilibration time of 3 min. All molecules of interest were monitored by mass spectrometric detection operating in multiple-reaction monitoring mode. The method was originally validated in human plasma based on the recommendations of regulatory agencies through tests of precision, accuracy, extraction recovery, identity confirmation, trueness, matrix effect, process efficiency, stability, selectivity, linearity and carry-over effect fulfilling the guideline requirements [54].

2.3. Surgical vagotomy

The surgical vagotomy procedure was performed as described [55,56]. Briefly, mice under isoflurane anesthesia were placed on their backs and an incision was made in the abdominal midline. The liver was then

moved carefully to the right exposing the esophagus. The vagus nerve was exposed and cauterized from the esophagus. The abdominal incision was then sutured with surgical silk. Sham surgeries were also performed, in which the nerve was exposed but not cauterized. The animals recovered for 1 week before other procedures. The effectiveness of the vagotomy was assessed at the end of the study by post-mortem analysis of the stomach. Only the mice that showed an evident increase in stomach size after vagotomy (due to motoric dysfunction) were included in the analysis [55].

2.4. Whole-brain magnetic resonance imaging (MRI)

MRI procedures were carried during the light period of the diurnal cycle in WT and PTP1B–KO mice in *ad libitum* conditions. Mice were anesthetized with isoflurane and remained under anesthesia during the procedure. Throughout the course of imaging acquisitions, isoflurane levels were kept in conditions that maintained the breathing rhythm between 40 and 70 breaths *per* min. Respiration rate was monitored using a sensor located below the abdomen, and body temperature through a rectal probe with a Biotrig physiological monitor (SA Instruments, Inc., Stony Brook, NY, USA). To avoid a decrease in animal temperature during MRI acquisition, the holder was covered with a heated blanket. MRI experiments were performed on a 7 T horizontal bore (16 cm diameter) superconducting magnet equipped with a ^{1}H selective birdcage resonator of 23 mm and a 90 mm diameter gradient insert (360 mT/m) (Biospec R 7T, Bruker Biospin, Ettlingen, Germany). Imaging data were acquired using a Hewlett-Packard console running Paravision 5.1 or 6.1 software (Bruker Medical Gmbh, Ettlingen, Germany). Specifically, 48 h after the intrahypothalamic injection of OLA, mice were anesthetized with isoflurane and underwent MRI acquisitions. MRI studies acquired T2 morphological images from all brain to identify the intrahypothalamic injected section. Furthermore, in mice under chronic i.p. treatment brain inflammation was inferred by the analysis of T2 maps which acquisition relied on a set of T2 images acquired.

2.5. Quantification of hepatic triglyceride (TG) synthesis fluxes and fatty acid composition

At the start of the dark period of the day before the sacrifice, mice were intraperitoneally injected with 4 ml/100 g body mass of 99.8% enriched $^{2}H_2O$ (Cambridge Isotopes Limited, Tewksbury, MA, USA) containing 9 mg/ml NaCl and the drinking water was enriched to 5% with $^{2}H_2O$. The following morning, the animals were euthanized and the blood was collected for plasma analysis of body water ^{2}H-enrichment by ^{2}H nuclear magnetic resonance (^{2}H NMR) spectroscopy. Liver was dissected and snap-frozen.

Extraction and purification of liver triglycerides (TGs): Frozen liver samples weighing between 0.5 and 1 g were powdered under liquid nitrogen and rapidly mixed with HPLC-grade methanol (4.6 ml/g) followed by methyl-tert-butyl ether (MTBE) (15.4 ml/g). The mixture was placed in a shaker for 1.5 h at room temperature then centrifuged at 13 000 g for 10 min. After centrifugation, the insoluble pellet containing hepatic glycogen was separated from the upper phase of the mixture. The upper phase was further separated into an aqueous fraction and an organic fraction. This upper phase contained the hepatic lipids. The organic fraction of the upper phase was dried under hood in an amber glass vial. TGs from the dried organic fraction were purified with a solid phase extraction (SPE) process as described [57]. Briefly, Discovery DSC-Si SPE cartridges (2 g/12 ml) were washed with 8 ml of hexane/MTBE (96/4; v/v) followed by 24 ml of hexane. The dried lipids were re-suspended in 500 μl of hexane/MTBE (200/3; v/v) and loaded into the column after washing. The lipid vials were washed with a further 500 μl of solvent to quantitatively transfer the lipids to the column. TGs were eluted with 32 ml of hexane/MTBE (96/4; v/v), collected in 4 ml fractions. Fractions containing TGs were identified by thin-layer chromatography. A few microliters of the eluted fractions were spotted on the TLC plate and the plate was developed with petroleum ether/-diethyl ether/acetic acid (7.0/1.0/0.1; v/v/v). After drying, lipid spots were visualized under iodine vapor. The TG-containing fractions were pooled, dried under hood and stored at −20 °C. For analysis of ^{2}H-enrichment and FA composition by NMR, each fraction was dissolved in 0.5 ml anhydrous ≥99% $CHCl_3$ with amylenes as stabilizer (Sigma-Aldrich, St. Louis, MO, USA) and pipetted into a 5-mm NMR tube. To this, 25 μl of a pyrazine standard enriched to 1% with pyrazine-d_4 and dissolved in $CHCl_3$ (0.07 g pyrazine/1 g $CHCl_3$), and 50 μl of C_6F_6were added.

NMR spectra acquisition and analysis: All NMR spectra were acquired with an 11.7 T Bruker Avance III HD system using a dedicated 5 mm ^{2}H -probe with a^{19}F-lock channel and ^{1}H-decoupling coil and a probe temperature of 25 °C. For analysis of triglyceride ^{2}H-enrichment, both ^{1}H and ^{2}H NMR spectra were acquired. ^{1}H spectra were obtained with a 90° pulse, 10 kHz spectral width, 3 s acquisition time, and 5 s pulse delay. Sixteen free-induction decays (f.i.d.) were collected for each spectrum. Fully relaxed ^{2}H NMR spectra were obtained with a 90° pulse, a 1230 Hz sweep width, an acquisition time of 0.67 s and a pulse delay of 8 s. Between 200 and 5000 f.i.d. were acquired for each spectrum. The summed f.i.d. was processed with 1 Hz line-broadening before Fourier transform.

All spectra were analyzed with ACD/NMR Processor Academic Edition software (ACD/Labs, Advanced Chemistry Development, Inc., Ontario, Canada).

2.6. Tissue sample collection

At week 8 (for the i.p. and oral gavage treatments), month 7 (for the oral dietary treatment) or 30 min, 8 h and 48 h post-injection (for the intrahypothalamic injection), mice were euthanized. Blood was collected with EDTA to prevent clotting, and immediately centrifuged for 20 min at 15 600 g. Plasma was collected, frozen and stored at −80 °C. The brain was removed from the skull and the hypothalamus was isolated and snap-frozen. The liver and BAT were dissected and snap-frozen. The brain and liver samples were placed in 4% (w/v) paraformaldehyde (PFA, 16005, Sigma-Aldrich) for paraffin inclusion.

2.7. Primary culture of mouse hepatocytes

Primary hepatocytes were isolated from untreated mice or mice treated with OLA or DMSO by two-step perfusion with collagenase as described [26,58]. Cells were plated in 6- or 12-well collagen IV (C3867-1VL, Sigma-Aldrich) pre-coated plates and cultured in medium containing DMEM and Ham's F-12 medium (1:1) with heat-inactivated 10% fetal bovine serum (FBS, 10270–106, Life Technologies, Carlsbad, CA, USA) supplemented with 2 mM glutamine (25030–024, Life Technologies), 15 mM glucose, 20 mM HEPES, 100 U/ml penicillin, 100 μg/ml streptomycin (15140–122, Life Technologies) and 1 mM sodium pyruvate (11360–039, Life Technologies) (attachment media) for 24 h. Primary mouse hepatocytes derived from non-treated mice were exposed *ex vivo* to different concentrations of OLA for 48 h in FBS-free DMEM (11966–025, Life Technologies) supplemented with 5.5 mM glucose.

2.8. Crystal violet staining for cell viability

Primary mouse hepatocytes derived from non-treated mice were exposed *ex vivo* to 12.5 μM OLA for 48 h and cell viability was assessed by crystal violet staining. Briefly, cells were fixed for 15 min with 4% PFA, washed with PBS and incubated for 20 min with a solution of 0.1% crystal violet (HT901; Sigma-Aldrich) in H_2O. Afterwards, wells were rinsed with tap water and air dried. Crystal violet was dissolved with a solution of 10% acetic acid and absorbance was measured at 590 nm.

2.9. Cell culture

GT1-7 hypothalamic neuron cell line: GT1-7 cell line (kindly provided by Prof. P. Mellon, University of California, CA, USA) are transformed from mouse hypothalamic neurosecretory cells [59]. Cells were grown in DMEM supplemented with 10% FBS, 2 mM glutamine (Life Technologies), 20 mM HEPES, 100 U/ml penicillin, 100 μg/ml streptomycin (Life Technologies). For experiments, 75×10^4 cells per well were seeded in 6-well plates and left to grow until 90% confluence was reached.

Immortalized astrocyte cell culture: An immortalized murine astrocyte cell line was kindly provided by Prof. A. Cuadrado (IIBm, Spain). Cells were grown in DMEM supplemented with 10% FBS, 20 mM HEPES, 100 U/ml penicillin, 100 μg/ml streptomycin (Life Technologies). For experiments, 10^5 cells per well were seeded cells in 6-well plates and left to grow until 90% confluence was reached.

Immortalized microglial cell culture: An immortalized murine microglia cell line was kindly provided by Prof. A. Cuadrado. Cells were grown in DMEM supplemented with 10% FBS, 2 mM glutamine, 20 mM HEPES, 100 U/ml penicillin, 100 μg/ml streptomycin. For experiments, 5×10^5 cells per well were seeded cells in 6-well plate and left to grow until 90% confluence was reached.

After reaching confluence, cells were then treated with OLA (12.5 μM) for different time periods ranging from 5 min to 24 h in serum-free medium. For treatments with N-acetylcysteine (NAC, 38520-57-9, Sigma-Aldrich), a JNK inhibitor (SP600125, 129-56-6, MedChemExpress, New Jersey, USA) or a PTP1B pharmacological inhibitor (iPTP1B, 539741, Merck, Darmstadt, Germany) cells were pre-treated for 2 h in serum-free medium before OLA treatment.

2.10. Protein extraction from cells and tissues

To obtain total cell lysates, cells were scraped off in lysis buffer (40 mM Tris-HCl, 5 mM EDTA, 30 μM sodium pyrophosphate tetrabasic ($Na_4P_2O_7$), 50 mM sodium fluoride (NaF), 100 mM sodium o-vanadate (Na_3VO_4), 1% Triton X-100, 1 mM phenylmethanesulfonyl fluoride (PMSF), and 10 μg/ml protease inhibitors cocktail, at final pH 7.4–7.6). Afterwards, samples were cleared by centrifugation (once at 13 600 g for 20 min at 4 °C for cell lines). Supernatants were stored at −20 °C. The protein concentration was measured by the Bradford dye (#5000006, Bio-Rad, Hercules, CA, USA) method using bovine serum albumin (BSA) as standard.

To extract total protein from tissues (hypothalamus, liver and BAT), samples were homogenized in ice-cold lysis buffer (50 mM HEPES, 1% Triton X-100, 50 mM $Na_4P_2O_7$, 0.1 M NaF, 10 mM EDTA, 10 mM $Na_4P_2O_7$, 1 mM PMSF, and 10 μg/ml of protease inhibitors cocktail, at final pH 7.4–7.6) using a polytron tissue homogenizer (0003737000, IKA, Staufen, Germany). Extracts were kept on ice during the process. Extracts were cleared by centrifugation at 40 000 g for 40 min at 4 °C, twice. Supernatants were then aliquoted and stored at −80 °C. Protein determination was performed by the BCA dye method using BCA Protein Assay Kit (23227, Thermo Fisher Scientific, Waltham, MA, USA) and BSA as standard.

2.11. Western blot

After protein content determination, samples were prepared with equal amount of protein, boiled at 98 °C for 5 min and analyzed by Western blot. After SDS-polyacrylamide gel electrophoresis (SDS-PAGE), gels were transferred to PVDF membranes (Millipore, Burlington, MA, USA) previously activated with 100% methanol for 5 min. After transferring, membranes were blocked using 4% non-fat dried milk in TTBS (10 mM Tris-HCl, 150 mM NaCl pH 7.5, Tween 20 (0.05% w/v)) for 2 h, and incubated overnight at 4 °C with the primary antibodies in TTBS. The membranes were then washed and incubated with the appropriated secondary antibody diluted in blocking solution. Immunoreactive bands were visualized in a ChemiDoc™ MP digital imager (Bio-Rad Bio-Rad) by using the Clarity Western ECL Substrate (#170–5061, Bio-Rad) or by X-ray film exposure. Experiments were quantified by densitometry using ImageJ software (National Institutes of Health (NIH), Bethesda, MD, USA).

2.12. Quantitative real-time PCR analysis (RT-qPCR)

Total RNA from tissues and cells was extracted with Tri reagent (AM9738, Life Technologies) and reverse transcribed using a SuperScript First-Strand Synthesis System (18080051, Life Technologies) for real time quantitative PCR (RT-qPCR) following the manufacturer's indications. RT-qPCR was performed with an ABI 7900 sequence detector (Applied Biosystems, Waltham. MA, USA). The primers sequences/probes are included in Supplementary Table 2.

2.13. Transcriptomic analysis by RNA sequencing

Livers from mice under dietary treatment were collected at sacrifice and snap frozen at −80 °C. Total RNA was extracted using the PureLink RNA Mini Kit (Life Technologies). Total RNA expression was analyzed using Illumina TruSeq Stranded RNASeq technology (Illumina, San Diego, CA, USA). The libraries were sequenced (2 × 100 bp) with a mean output of 40 million reads in a NovaSeq 6000 sequencer (Illumina). After a quality control check with FastQC (www.bioinformatics.babraham. ac.uk/projects/fastqc, access date 27 May 2019), the reads were aligned to reference transcripts with the Kallisto algorithm [60], which provides a matrix of estimated counts per transcript as the output. Exploratory analyses included principal component analysis (PCA) and hierarchical clustering (HC). Transcriptomic analyses were performed with the DESeq2 package [61], for which differentially expressed genes (DEGs) were described as those with an adjusted p-value (p-adj) of <0.1 when performing a Wald test between two conditions and a Benjamini–Hochberg adjustment. Overrepresentation analyses (ORAs) of the DEGs were completed with the WEB-based GEne SeT AnaLysis Toolkit (WebGestalt) [62]. The raw data was submitted to the Gene Expression Omnibus (GEO) database with the reference GSE222697.

2.14. Tissue histological analysis, immunohistochemistry, immunofluorescence and MitoTracker red CM-H_2Xros staining

Immunohistochemistry: Tissue sections (5 μm) were de-waxed and rehydrated through a descending series of ethanol dilutions (100, 96, 75, 50%). Antigen retrieval was achieved by microwaving for 5 min at 600 W in 100 mM citrate buffer (pH 6) with 0.05% (w/v) Tween-20, followed by three washes in PBS. Tissue sections were permeabilized with PBS-Triton X-100 (0.3% w/v; T8787, Sigma-Aldrich). Non-specific binding was blocked with 3% (v/v) horse serum (H0146, Sigma-Aldrich) in PBS-Triton X-100 (0.3% v/v). Sections were incubated overnight at 4 °C with primary antibodies in blocking buffer and then incubated with a biotinylated secondary antibody combined with streptavidin-HRP by the ABC (Avidin Biotin Complex) method (Vectastain® Elite® ABC-HRP Kit, PK-6100, Vector Laboratories, Newark, CA, USA). DAB Substrate kit (416424, Palex Medical SA., Madrid, Spain) was used following the manufacturer's instructions. Images were collected with an Axiophot light microscope (Carl Zeiss, Oberkochen, Germany).

Oil-Red O (ORO) Staining: For ORO staining, liver sections were fixed overnight with 4% PFA and cryoprotected in subsequent gradients of 15 and 30% sucrose (in PBS) at 4 °C. Afterwards, samples were frozen in Tissue-Tec OCT (Sakura Finetek USA, Torrance, CA, USA) and sectioned at 5 μm using a Leica CM3050 S cryostat. Tissue slides were then left at room temperature for 10 min and the remaining OCT was washed with PBS. Slides were then placed in isopropanol 60% for 15 s before of filtered ORO (O0625, Merck) solution (60% isoropranol in water) for 15 min. After washing the slides with PBS, they were stained with Carazzi's hematoxylin for 1 min. The excess of the hematoxylin was

washed with PBS, after which the slides were mounted in 50% glycerol (in PBS) and sealed. After drying, the images were collected with an Axiophot light microscope (Carl Zeiss).

Immunofluorescence in tissue sections: After rehydrating and antigen retrieval, non-specific binding was blocked with 0.5% (w/v) BSA (MB04602, NZYTech, Lisbon, Portugal) in PBS-Triton X-100 (0.3% v/v). Sections were incubated overnight at 4 °C with the primary antibody in blocking buffer and then incubated with the appropriated fluorescent secondary antibody. Nuclei were stained for 5 min with 4,6-diamidino-2-phenylindole (DAPI) in PBS (1:1000) and sections were mounted in Fluoromont (Sigma-Aldrich). Samples were analyzed using the optical Nikon N91 fluorescence microscope (Carl Zeiss) or confocal microscopy (Carl Zeiss).

***MitoTracker Red CM-H_2Xros* staining**: GT1-7 neuron cells were incubated with MitoTracker Red CM-H_2Xros (M7513, Thermo Fisher Scientific) for 4 min in darkness at 37 °C. Cells were fixed with 3% PFA and 1.5% glutheraldehyde as described in Ref. [63] for 5 min, time at which the fixative was replaced by PBS and the cells were observed by confocal microscopy (Carl Zeiss).

TUNEL staining: Slides from mice brain were used for the detection of cell death induced by the treatment with OLA by using the DeadEnd™ Fluorometric TUNEL System (G3250, Promega, Madison, WI, USA) according to supplier's instructions. Briefly, tissue sections (5 μm) were dewaxed by two washes with xylene and rehydrated through a descending series of ethanol dilutions (100, 95, 85, 75, 50%) and washed with 0.85% NaCl. The slides were then fixed 15 min with 4% PFA before permeabilization with Proteinase K treatment (20 μg/ml for 10 min), after which the samples were fixed again for 5 min with 4% PFA before 10 min incubation in equilibration buffer (EB). The dead cells were then labeled with a mix of 1:10 nucleotides and 1:50 of Terminal deoxynucleotidyl transferase (Tdt) enzyme in EB for 60 min at 37 °C, avoiding light exposure and covered with a plastic slip. The reaction was stopped by washing the preparations in 2x saline-sodium citrate (SSC) buffer. Nuclei were stained for 5 min with DAPI in PBS (1:1000) and sections were mounted in Fluoromont (Sigma-Aldrich) and images were collected by confocal microscopy (Carl Zeiss).

2.15. Determination of hepatic ATP content

Around 50 mg of the liver were homogenized with the polytron tissue homogenizer in 6% (v/v) $HClO_4$ and left overnight at 4 °C under rotation. Then, samples were neutralized with 6 M KOH and centrifuged at 9300 g for 10 min at 4 °C. ATP content in the supernatants was determined with the bioluminescence ATP determination kit (PRO LBR-PO10, Biaffin GMbH & Co. KG, Kassel, Germany) following manufacturer's instructions. The chemiluminescence generated was detected at a 560 nm wavelength in a GloMax 96 Microplate luminometer (Promega). A standard curve with increasing concentrations of ATP was used to calculate the amount of ATP in each sample. The values were normalized for the specific tissue amount (in mg) used for each sample.

2.16. Analysis of TG levels in plasma and liver samples

The hepatic lipid extraction and purification was adapted from Blight et al. [64]. Around 50 mg of liver samples were homogenized in 20 mM potassium phosphate buffer pH 7.4 with the Polytron. Homogenates were incubated with a mixture of chloroform/methanol (1:1) in rotation at RT for 1 h. Afterwards, chloroform and 0.74% (w/v) KCl were added, followed by centrifugation at 500*g* for 5 min. A three-phase mixture was obtained; the down phase was collected, mixed with chloroform/methanol (1:1) and centrifuged at 500 g for 5 min at 4 °C. Then, the lower phase was collected and evaporated. Pellets containing hepatic lipids were dissolved in isopropanol and triglycerides were quantified with a colorimetric kit (11528–11529, Biosystems, Barcelona, Spain). The values were normalized to mg of tissue. Plasma TGs levels were measured by using the same colorimetric kit following the manufacturer's instructions.

2.17. Metabolomic analysis of the hypothalamus

Extraction of metabolites from the hypothalamus: Snap-frozen hypothalamus (5–10 mg) were processed in Biosfer Teslab (Tarragona, Spain) for metabolomic and lipidomic analysis. Metabolites were extracted from the hypothalamus by using a modified version of the BUME method [65], as previously described [66]. An aqueous and a lipid-enriched phases were obtained. The upper lipid-enriched phase was carefully dried in a *Speedvac* system, until evaporation of organic solvents, and reconstituted in a solution of $CDCl_3$:CD_3OD:D_2O (16:7:1, v/v/v) containing Tetramethylsilane (TMS). The lower aqueous phase was completely dried in a nitrogen stream and reconstituted in a solution of D_2O containing 2.32 mM trisilylpropionic acid (TSP). Aqueous and lipid phases were transferred into 5-mm NMR tubes.

NMR measurements: Aqueous and lipid-enriched extracts were measured using an Avance III-600 Bruker spectrometer operating at proton frequency of 600 MHz. For the lipidomic analysis, a 90° pulse with water presaturation sequence (zgpr) was used. For aqueous extracts, one-dimensional ^{1}H pulse experiments were carried out using the nuclear Overhauser effect spectroscopy (NOESY)-presaturation sequence to suppress the residual water peak at around 4.7 ppm.

NMR data analysis: The frequency domain spectra obtained were phased, baseline-corrected and referenced to TSP or TMS signals ($\delta = 0$ ppm) using TopSpin software (Bruker Daltonics). Quantification of lipid-related signals was carried out with an adaptation of LipSpin[2] by an in-house software. Quantification of signals from the aqueous phase was carried out with an adaptation of Dolphin procedure [67] by using an *in-house* software. Resonance assignments for both phases were performed based on the literature, Chenomx and HMDB [68].

2.18. Tissue molecular imaging by LDI-MS

Tissue imaging by laser desorption/ionization–mass spectrometry (LDI–MS) imaging was performed as previously described [69,70]. Briefly, gold nanolayers were deposited over the 10 μm tissue sections using the ATC Orion 8-HV sputtering system (AJA International, N. Scituate, MA, USA), and LDI–MS tissue images were acquired using a Spectroglyph MALDI source coupled to an Exploris 120 Orbitrap (Thermo Fisher Scientific) LDI-MS working in positive ionization mode (range *m/z* 100–1500). Three biological replicates (*i.e.*, three male mice per group) were used for tissue molecular imaging by LDI-MS. Molecular images were acquired at 25 μm lateral and 120 000 spectral resolutions (FWHM at *m/z* 200). Data processing and visualization was based on the workflow described by Ràfols et al. [70] using the open-source software rMSI [71] and rMSIproc [72]. Lipid identification was based on the exact mass of their positive adducts according to the LIPID MAPS [73] (filtering at 0.005 Da).

2.19. Data analysis

Statistical analysis was performed with GraphPad Prism version-7.0 (GraphPad Software, San Diego,CA, USA). Data are reported as mean and standard error of the mean (SEM). Comparisons between groups were made using Student's *t*-test if two groups were considered. If more than 2 groups were studied with one variable taken in consideration (*i.e.,* treatment or genotype) One Way-ANOVA ($\alpha = 0.05$) was used, with Bonferroni's post-hoc test carried for multiple comparisons between the groups. Moreover, when more than one variable was compared (*i.e.,* treatment and genotype) the data were analyzed with Two Way-ANOVA ($\alpha = 0.05$) with multiple comparisons done with Bonferroni's post-hoc test. If not mentioned in the figure legend, it must be considered that Two Way-ANOVA with Bonferroni's test was used for the presented analysis. In Supplementary Table 4, fold changes and *p*-values were calculated using 1000 random pixels from each LDI-MS sample (each

sample containing between 2431 and 22 844 pixels). Fold change was calculated as the log2 (average intensity of group 2/average intensity of group 1) and the *p*-values were calculated using Kruskal-Wallis test adjusted for multiple comparisons.

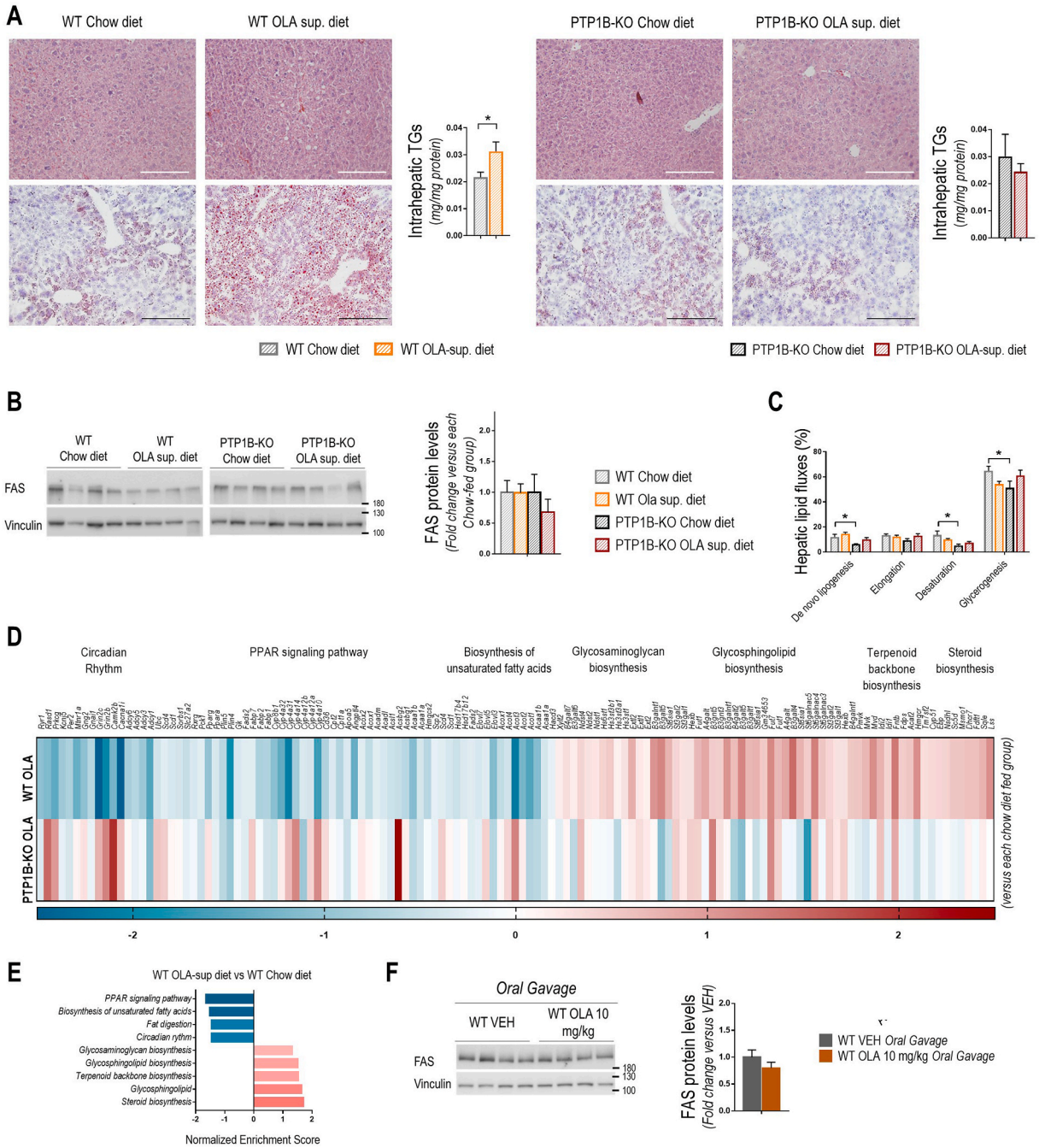

Fig. 1. OLA dietary treatment promoted intrahepatic lipid accumulation in WT, but not in PTP1B–KO male mice. **A.** Representative images of liver sections with H&E (20x, scale bars-100 μm) (WT Chow diet: n = 3; WT OLA sup. diet: n = 3; PTP1B–KO Chow diet: n = 3; PTP1B–KO OLA sup. diet: n = 3) and ORO staining (WT Chow diet: n = 4; WT OLA sup. diet: n = 4; PTP1B–KO Chow diet: n = 4; PTP1B–KO OLA sup. diet: n = 4) and intrahepatic TGs (WT Chow diet: n = 9; WT OLA sup. diet: n = 9; PTP1B–KO Chow diet: n = 6; PTP1B–KO OLA sup. diet: n = 7, groups were compared using *Student's t-test*). **B.** Representative Western blot images of hepatic FAS with densitometric quantification normalized for Vinculin protein levels (WT Chow diet: n = 12; WT OLA sup. diet: n = 12; PTP1B–KO Chow diet: n = 12; PTP1B–KO OLA sup diet: n = 12). **C.** Quantification of hepatic lipid fluxes (WT Chow diet: n = 9; WT OLA sup. diet: n = 9; PTP1B–KO Chow diet: n = 6; PTP1B–KO OLA sup. diet: n = 7). **D.** RNAseq data: heatmap of hepatic gene expression comparing WT or PTP1B–KO mice fed an OLA supplemented diet *versus* each genotype-matched control group (fed a chow diet). The $\log_2$(fold change) for each gene is presented. **E.** Principal categories of steatosis-related gene families regulated in WT mice fed an OLA supplemented diet in comparison to WT mice fed a chow diet. **F.** WT male mice received a daily oral gavage of OLA (10 mg/kg) or VEH during 8 weeks. Representative Western blot images of FAS protein levels in liver and densitometric quantification normalized for Vinculin protein levels (WT VEH: n = 6; WT OLA: n = 6, groups were compared using *Student's t-test*). Each point/bar corresponds to mean ± SEM; comparisons between groups: *p < 0.05.

3. Results

3.1. Differential effects of OLA i.p. and dietary treatment in intrahepatic lipid accumulation and FAS levels in WT and PTP1B–KO male mice

Since our previous study [32] showed that WT mice under treatment with OLA supplemented in the diet gained more weight compared with mice fed a regular chow diet, while PTP1B–KO mice were protected against weight gain, we investigated whether weight gain in WT mice was associated with intrahepatic lipid accumulation. As shown in the representative H&E and ORO stained liver sections from both genotypes (Fig. 1A and Supplementary Fig. 1A), increased hepatic lipid content and TG levels were found exclusively in WT mice receiving OLA orally (Fig. 1A). However, hepatic FAS protein levels remained unchanged regardless diet or genotype (Fig. 1B). The analysis of hepatic lipid fluxes in mice receiving $^{2}H_2O$ 16 h prior the sacrifice revealed no differences in *de novo* lipogenesis, FA elongation and desaturation or glycerogenesis (Fig. 1C). Altogether, these results suggest that intrahepatic lipid accumulation upon OLA dietary treatment does not rely on *de novo* lipogenesis. Of note, decreases in *de novo* lipogenesis, desaturation and glycerogenesis were found in PTP1B–KO mice under chow diet compared to WT mice.

We conducted RNAseq transcriptomic analysis in livers from mice at the end of the OLA dietary treatment. As shown in Fig. 1D, OLA differentially impacted hepatic gene expression in mice depending on the genotype, being substantial changes in steatosis-related gene families evident only in WT mice (Fig. 1E). Since, our previous work showed that WT mice fed an OLA-supplemented diet presented hyperphagia [32], the intrahepatic lipid accumulation is likely due to the augmented caloric intake rather than enhanced *de novo* lipogenesis. To substantiate these results, another cohort of mice was treated with OLA (10 mg/kg/day) by oral gavage for 8 weeks. As observed in the dietary treatment, OLA administration by gavage did not alter FAS protein levels (Fig. 1F).

Next, histological analysis was performed in liver sections from WT and PTP1B–KO mice administered OLA via i.p. that, as shown in our previous study [32], lost weight. As expected, no features of hepatic steatosis were observed and hepatic TG content remained unchanged (Fig. 2A and Supplementary Fig. 1B). Unexpectedly, in WT mice treated with OLA via i.p., FAS protein levels were increased (Fig. 2B) in parallel with its mRNA levels (Fig. 2C). This effect was associated with reduced *Insig2* and increased *Srebf1* mRNAs (encoding INSIG2 and SREBP1c, respectively), both transcriptional regulators of the *Fasn* gene (Fig. 2C). Moreover, no changes in *Insig1* mRNA levels were found. In those mice, decreased hepatic ATP levels were found (Fig. 2D) in parallel to an increase in AMPK phosphorylation and, in turn, in the inhibitory phosphorylation of its downstream effector ACC (Fig. 2E). Similar effects in AMPK/ACC phosphorylation and FAS levels were found in primary hepatocytes isolated from OLA-treated mice (Fig. 2F). By contrast, PTP1B-deficient male mice did not present these alterations in the liver or primary hepatocytes. Altogether, these results led us to propose that an OLA i.p. treatment or the inhibition of PTP1B could be beneficial in preventing fat accumulation in the liver associated with the OLA oral treatment.

To test if OLA upregulates FAS expression in a cell autonomous manner, primary hepatocytes were treated *ex vivo* for 48 h with OLA at different concentrations. As shown in Fig. 2G, the highest concentration (12.5 μM) did not compromise hepatocyte cell viability and also did not increase the lipid content by ORO staining. Moreover, no differences in FAS or phospho-ACC levels were observed (Fig. 2H, Supplementary Fig. 1C), pointing to an inter-organ crosstalk in the modulation of FAS expression in the liver by OLA.

3.2. Hypothalamic JNK phosphorylation controls hepatic FAS levels in WT male mice treated with OLA via i.p.

Based on the previously reported relevance of hypothalamic JNK in controlling FAS expression in the liver in the context of the central effects of thyroid hormones [19], we determined JNK phosphorylation in the hypothalamus of mice treated via i.p. that presented elevated OLA levels in this brain region compared to those of the oral treatment [32]. Fig. 3A shows increased hypothalamic phospho-JNK in WT, but not PTP1B–KO mice, upon OLA i.p. administration, despite comparable OLA levels in the hypothalamus (132.75 ± 17.80 ng/ml in WT mice as reported [32] and 105.00 ± 10.46 ng/ml in PTP1B–KO, $p = 0.2781$) and plasma (207.04 ± 16.23 ng/ml in WT as reported [32] and 182.28 ± 14.40 ng/ml in PTP1B–KO, $p = 0.2820$) measured 2 h after the OLA injection. Moreover, this effect was absent in the hypothalamus of mice fed an OLA-supplemented diet (Supplementary Fig. 2A) or mice treated by oral gavage (Supplementary Fig. 2B). To substantiate these results, we tested the direct effect of OLA in activating JNK in different cell types of the hypothalamus. As shown in Fig. 3B, OLA (12.5 μM) increased phospho-JNK in immortalized GT1-7 hypothalamic neurons, microglia and astrocytes.

To further investigate the direct effect of OLA in modulating JNK phosphorylation in the hypothalamus and, hence, hepatic FAS levels, WT mice received an intrahypothalamic injection of OLA and after 30 min, 8 and 48 h, the hypothalami were collected. As shown in Fig. 3C and D, hypothalamic phospho-JNK was increased 30 min after the injection, while the elevation in hepatic FAS levels was observed at 48 h. However, no changes were found at either time point in phospho-ACC or phospho-AMPK in the liver of those mice (Fig. 3E), suggesting a direct connection between JNK activation in the hypothalamus and FAS upregulation in the liver by OLA.

To investigate the relevance of the vagus nerve on the central effects driven by OLA in hepatic metabolism, OLA was injected in the hypothalamus of sham-operated or vagotomized C57BL/6J male mice. Only the mice that showed an evident increase in stomach size after vagotomy (due to motoric dysfunction) were included in the analysis (Supplementary Fig. 2C) [55,56]. In vagotomized mice, the single intrahypothalamic injection of OLA did not alter FAS expression in the liver, supporting that OLA-mediated modulatory signals are likely transmitted from the CNS to the liver through the vagus nerve (Fig. 3F).

Next, we conducted experiments in a cohort of mice in which JNK was deleted specifically the hypothalamus by injecting AAV-Cre particles in the VMH of mice with global JNK2 deletion (JNK2-KO/JNK1$^{flox-flox}$) [19] prior to OLA i.p. treatment (10 mg/kg/day) for 8 weeks. Fig. 4A shows the deletion of JNK1/2 isoforms in the hypothalamus. Importantly, this deletion prevented OLA-induced FAS upregulation in the liver (Fig. 4B). These data support the relevance of JNK1 activation status in the hypothalamic control of hepatic FAS in response to OLA i.p. treatment. By contrast, parameters such as body weight loss, BAT and tail temperature, as well as BAT UCP-1 levels were similar in OLA-treated mice regardless the absence of JNK1 in the hypothalamus (Fig. 4C and E), pointing that hypothalamic JNK1 does not control BAT thermogenesis upon OLA i.p. treatment.

Since, on the one hand, Martinez-Sanchez et al. [19] reported that, in the context of central T_3 administration, the reduction of hypothalamic AMPKα1 activates JNK in this brain region and, on the other, our previous work [32] demonstrated that i.p. or central OLA administration reduces AMPK phosphorylation in the hypothalamus, we assessed if preventing this effect impacts on OLA-induced JNK phosphorylation (Fig. 3C). To achieve this, mice injected AAV expressing a constitutively active version of AMPKα1 directly in the VMH received a single intrahypothalamic injection of OLA or DMSO. As shown in Fig. 4F, under this condition OLA was able to increase hypothalamic JNK phosphorylation, supporting an AMPK-independent effect in this response.

In our previous study, we demonstrated that upon a single administration, hypothalamic and plasma OLA levels are almost 2.5-fold

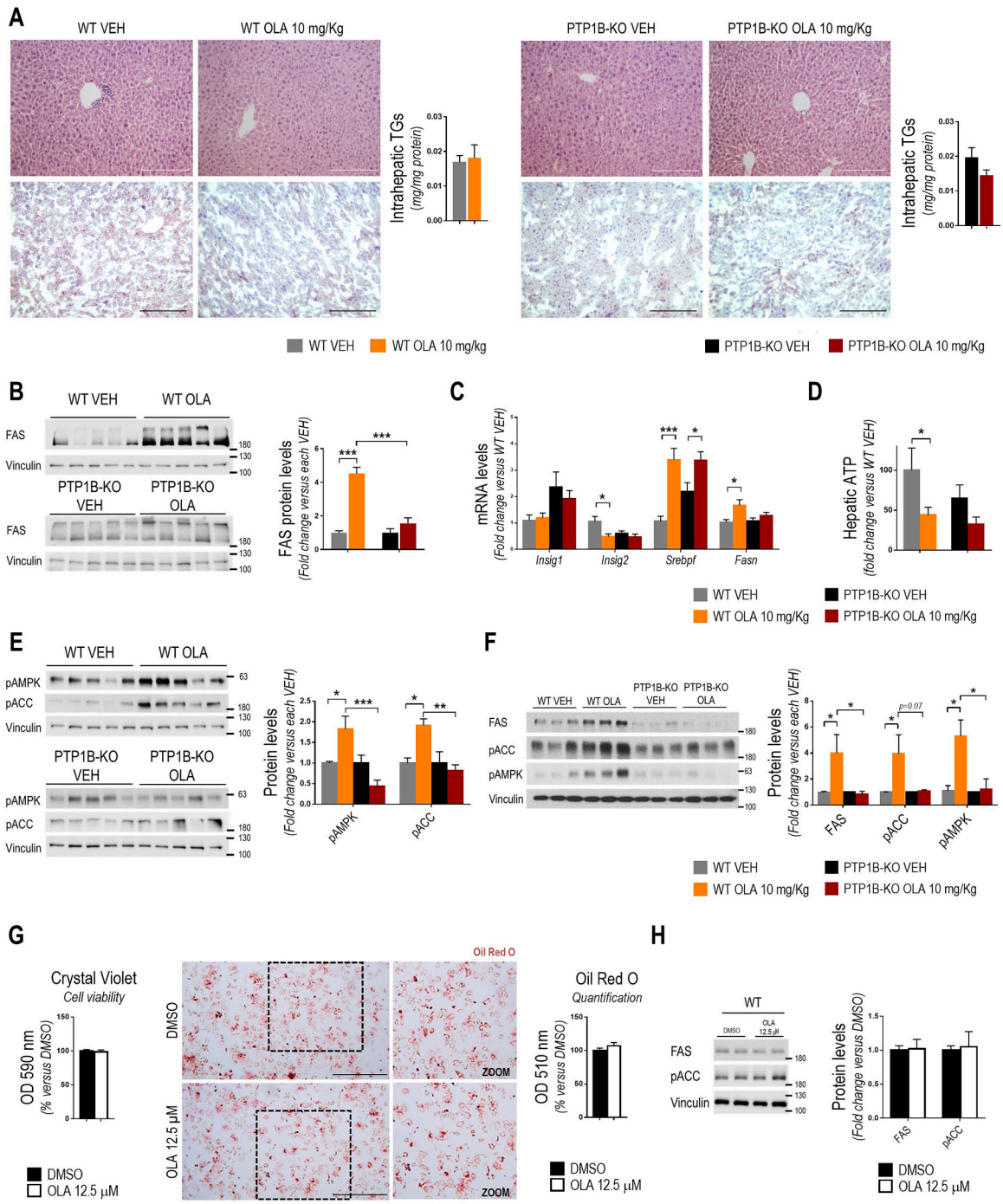

Fig. 2. OLA i.p. administration prevented intrahepatic lipid accumulation in WT and PTP1B–KO male mice despite of FAS upregulation found in WT mice. WT and PTP1B–KO male mice received a daily i.p. injection of OLA (10 mg/kg) during 8 weeks. **A.** Representative images of liver sections with H&E (20x, scale bars-100 μm) (WT VEH: n = 3; WT OLA: n = 3; PTP1B–KO VEH: n = 3; PTP1B–KO OLA: n = 3) and ORO staining (WT VEH: n = 3; WT OLA: n = 3; PTP1B–KO VEH: n = 3; PTP1B–KO OLA: n = 3) and intrahepatic TGs (WT VEH: n = 4; WT OLA: n = 5; PTP1B–KO VEH: n = 8; PTP1B–KO OLA: n = 9, groups were compared using *Student's t-test*). **B.** Representative Western blot images of hepatic FAS and densitometric quantification normalized for Vinculin protein levels (WT VEH: n = 5; WT OLA: n = 5; PTP1B–KO VEH: n = 7; PTP1B–KO OLA: n = 6). **C.** *Fasn, Insig1*, *Insig2* and *Srebf1* mRNA levels using *Tbp* and *Actb* as housekeeping genes (WT VEH: n = 5; WT OLA: n = 5; PTP1B–KO VEH: n = 7; PTP1B–KO OLA: n = 8). **D.** ATP levels in livers of male mice from both genotypes (WT VEH: n = 15; WT OLA: n = 18; PTP1B–KO VEH: n = 10; PTP1B–KO OLA: n = 14). **E.** Representative Western blot images of hepatic ACC and AMPK phosphorylation and densitometric quantification normalized for Vinculin protein levels (WT VEH: n = 4–5; WT OLA: n = 5; PTP1B–KO VEH: n = 6–7; PTP1B–KO OLA: n = 5–6). **F.** Representative Western blots of FAS and ACC and AMPK phosphorylation in primary hepatocytes from OLA-treated mice and densitometric quantification normalized for Vinculin protein levels (WT VEH: n = 3–4; WT OLA: n = 3–4; PTP1B–KO VEH: n = 3; PTP1B–KO OLA: n = 3). **G.** Cell viability of mouse primary hepatocytes treated *in vitro* with OLA for 48 h (12.5 μM) using the crystal violet method (DMSO: n = 5; OLA: n = 5, groups were compared using *Student's t-test*) (left panel). ORO staining (middle panel, 5x, scale bars-2 mm) and respective zoom and the corresponding quantification in mouse primary hepatocytes treated OLA for 48 h (12.5 μM) (DMSO: n = 5; OLA: n = 5, groups were compared using *Student's t-test*) (*left panel*). **H.** Representative Western blot images of FAS and pACC protein levels of mouse primary hepatocytes treated as detailed in G. Densitometric quantification normalized for Vinculin protein levels (n = 4). Each point/bar corresponds to mean ± SEM; comparisons between groups: *$p < 0.05$; **$p < 0.01$; ***$p < 0.001$. (For interpretation of the references to color in this figure legend, the reader is referred to the Web version of this article.)

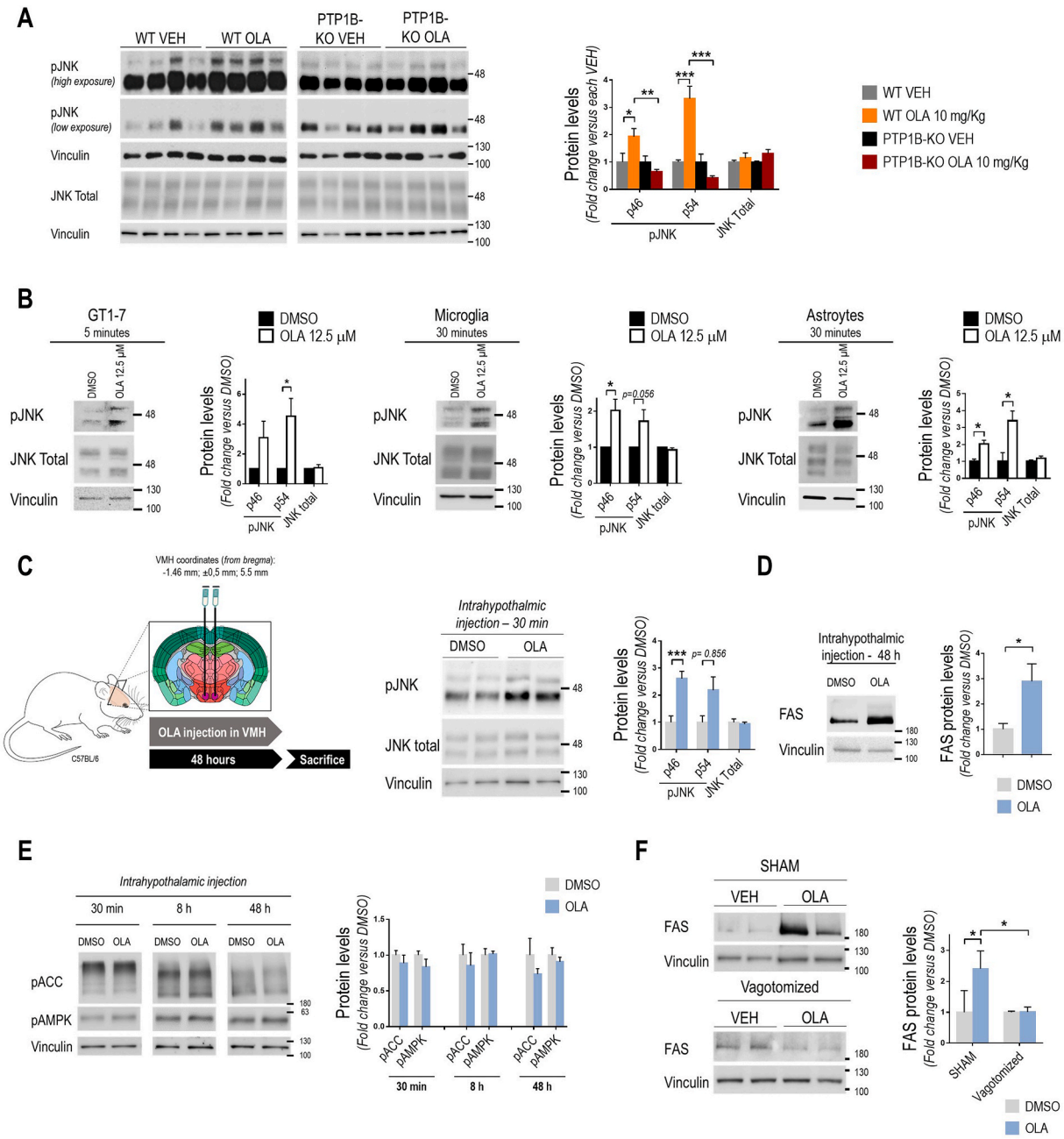

Fig. 3. Hypothalamic JNK phosphorylation paralleled with increased hepatic FAS levels in WT male mice treated with OLA via i.p. **A.** Representative Western blot images of hypothalamic JNK phosphorylation and total JNK and densitometric quantification normalized for total JNK and Vinculin protein levels, respectively (WT VEH: n = 4; WT OLA: n = 7; PTP1B–KO VEH: n = 6; PTP1B–KO OLA: n = 7). **B.** Representative Western blot images of JNK phosphorylation and total JNK in GT1-7 hypothalamic neurons (12.5 μM, 5 min, DMSO: n = 3; OLA: n = 3 independent experiments, groups were compared using *Student's t-test*), microglia (12.5 μM, 60 min, DMSO: n = 5; OLA: n = 5 independent experiments, groups were compared using *Student's t-test*) and astrocytes (12.5 μM, 60 min, DMSO: n = 3; OLA: n = 3 independent experiments, groups were compared using *Student's t-test*) treated with OLA. Densitometric quantification of phospho-JNK and total JNK normalized for total JNK and Vinculin protein levels, respectively. **C.** Experimental design (*left panel*). Representative Western blot images of hypothalamic JNK phosphorylation and total JNK in WT male mice 30 min after receiving an intrahypothalamic injection with OLA (15 nmol) (*middle panel*). Densitometric quantification of phospho-JNK and total JNK normalized for total JNK and Vinculin protein levels, respectively (*right panel*) (DMSO: n = 7; OLA: n = 9, groups were compared using *Student's t-test*). **D.** Representative Western blot images of hepatic FAS in WT male mice 48 h after receiving an intrahypothalamic injection with OLA (15 nmol) and densitometric quantification normalized for Vinculin levels (WT DMSO: n = 7; WT OLA: n = 10, groups were compared using *Student's t-test*). **E.** Representative Western blot images of hepatic pACC and pAMPK in WT male mice 30 min, 8 and 48 h after receiving an intrahypothalamic injection with OLA (15 nmol) and densitometric quantification normalized for Vinculin levels (30 min: WT DMSO: n = 7; WT OLA: n = 8; 8 h: WT DMSO: n = 3; WT OLA: n = 3; 48 h: WT DMSO: n = 5; WT OLA: n = 7, groups were compared using *Student's t-test*). **F.** WT male mice were vagotomized 7 days prior to OLA (15 nmol) intrahypothalamic injection and after 48 h livers were collected. Representative Western blot images of hepatic FAS and densitometric quantification normalized for Vinculin levels (Sham: DMSO: n = 3; OLA: n = 4; Vagotomized: DMSO: n = 6, OLA: n = 6). Each point/bar corresponds to mean ± SEM; comparisons between groups: *p < 0.05; **p < 0.01; ***p < 0.001.

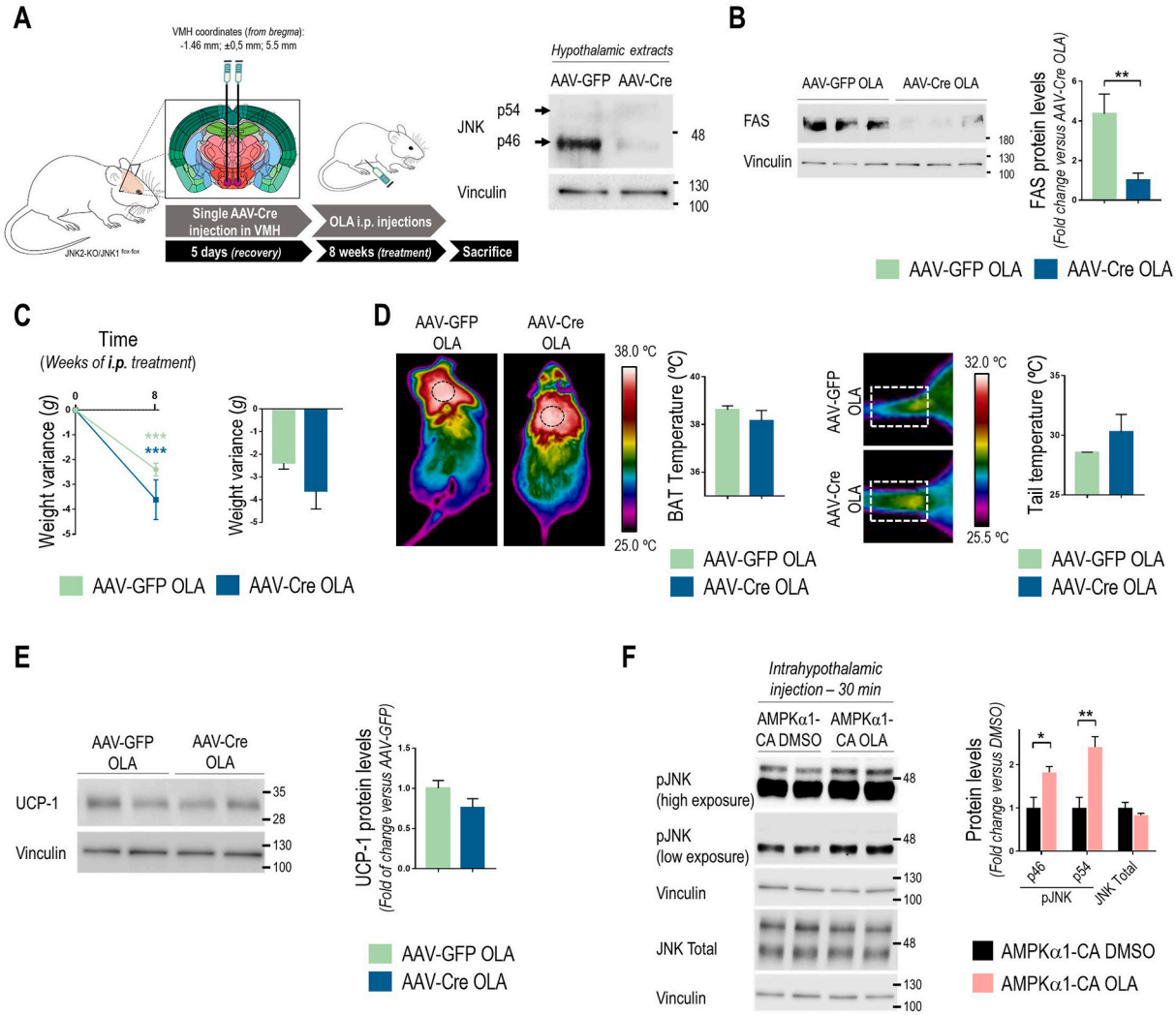

Fig. 4. JNK1 deletion prevented OLA-induced FAS upregulation in the liver. **A.** Experimental design of the intrahypothalamic injection of adeno-associated viruses encoding Cre recombinase in C57BL/6J male JNK2-KO/JNK1$^{flox\text{-}flox}$ mice 4 days prior to OLA i.p. daily injections for 8 weeks after which hypothalamus and liver were collected. Representative Western blot images of hypothalamic total JNK and Vinculin protein levels. **B.** Representative Western blot images of hepatic FAS in mice treated as in A, and densitometric quantification normalized for Vinculin levels (AAV-GFP OLA: n = 8; AAV-Cre OLA: n = 7, groups were compared using *Student's t-test*). **C.** Body weight variance at the beginning (week 0) and end (week 8) of the OLA i.p. treatment (AAV-GFP: n = 8; AAV-Cre: n = 8) (*left panel*). Body weight variance at the end of the OLA i.p. treatment (AAV-GFP: n = 8; AAV-Cre: n = 8, groups were compared using *Student's t-test*) (*right panel*). **D.** Thermographic pictures and quantification of BAT (*left panel*) and tail (*right panel*) maximal temperature of male mice via i.p. with OLA (AAV-GFP: n = 4; AAV-Cre: n = 4, groups were compared using *Student's t-test*). **E.** Representative Western blot of BAT UCP-1 and densitometric quantification normalized for Vinculin levels in mice treated with OLA via i.p. (AAV-GFP: n = 13; AAV-Cre: n = 12, groups were compared using *Student's t-test*). **F.** Representative Western blot of hypothalamic phospho-JNK protein levels in male mice injected AMPKα1-CA or GFP adenoviruses 5 days prior to OLA or DMSO intrahypothalamic injection for 30 min before sampling and respective densitometric quantification normalized for Vinculin levels (AMPKα1-CA VEH: n = 4; AMPKα1-CA OLA: n = 5, groups were compared using *Student's t-test*). Each point/bar corresponds to mean ± SEM; comparisons between groups: *p < 0.05; **p < 0.01; ***p < 0.001.

higher when OLA is administered via i.p. compared to oral gavage [32]. This result raises the hypothesis that, as occurred with AMPK, a threshold of OLA reaching the hypothalamus must be achieved to modulate JNK activation in this brain region, which is likely not overcome by the oral treatment. Thus, to understand if the modulation of JNK phosphorylation relays on hypothalamic OLA levels, mice were treated with OLA via i.p. injection at 5 mg/kg/day that, as previously shown [32], results in similar peaks of OLA levels in plasma and hypothalamus to those reached in the oral administration. As expected, mice receiving chronic treatment with OLA via i.p. at 5 mg/kg/day did not show increases in hypothalamic phospho-JNK and neither in hepatic FAS nor phospho-ACC (Supplementary Figs. 2D and 2E). These results support that the levels of OLA reaching the hypothalamus are also crucial for activating JNK in this brain region which, in turn, drives FAS upregulation in the liver.

3.3. OLA decreases antioxidant metabolites and increases lipid peroxidation in the hypothalamus of WT male mice treated with OLA via i.p.

The induction of hypothalamic JNK phosphorylation found in WT mice upon OLA i.p. treatment might be related to an increase in oxidative stress and/or inflammation. To test this, metabolomic and lipidomic studies of the hypothalamus were performed. A detailed analysis of a broad spectrum of small molecular weight metabolites revealed a significant decrease in those with antioxidant properties such as choline, glycine, acetate, N-acetylaspartate and sn-Glycero-3-phosphocholine [74–83] in the hypothalamus of OLA-treated WT male mice in comparison to the control mice receiving VEH, whereas no statistically differences were found in the levels of these metabolites in the hypothalamus of PTP1B–KO mice (Fig. 5A). By contrast, no

differences in the total levels of lipid species between VEH and OLA-treated mice within each genotype were found (Fig. 5B). Of interest, under basal conditions (VEH-treated), constitutively higher levels of several lipid species including glycerophospholipids (GLP), phosphatidylcholine (PC), sphingomyelin (SM), phosphatidylethanolamine (PE), cholesterol, polyunsaturated FA (PUFA)-2, −3 and −4 and total, omega (ω)9, ω6+ω7, ω3, docosahexaenoic acid (DHA) and arachidonic plus eicosapentaenoic acid (ARA+EPA) were found in the hypothalamus of PTP1B–KO mice when compared to their WT counterparts (Supplementary Fig. 4C). Among these species, GLP, PC, SM, PE, some PUFAs and ωs, DHA and EPA have antioxidant/anti-inflammatory properties [84–91]. To further assess the impact of the reduction of antioxidant metabolites in the hypothalamus of WT mice by OLA i.p. administration, we analyzed oxidative stress markers in tissue sections. As shown in the

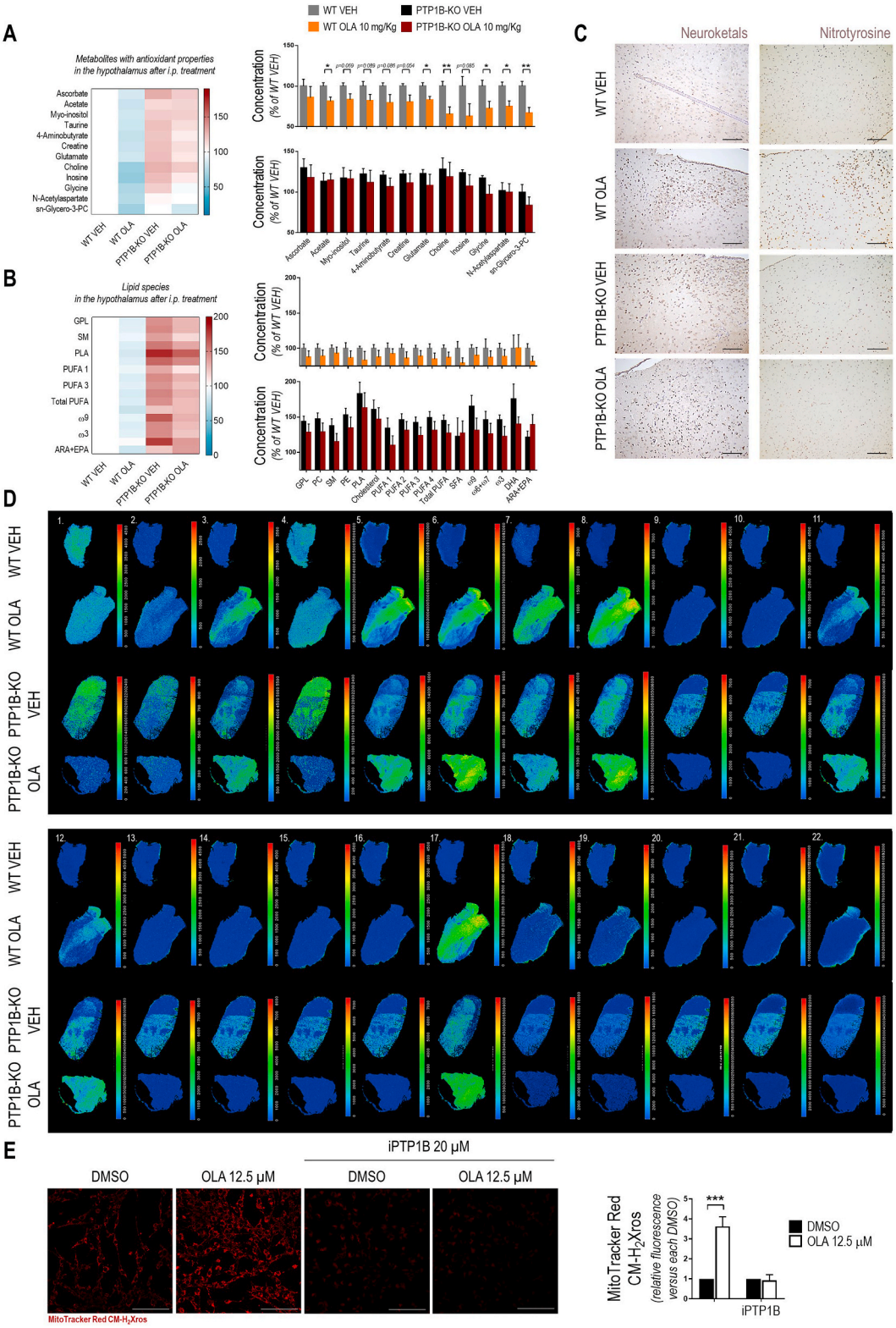

(caption on next page)

Fig. 5. OLA i.p. administration decreases antioxidant metabolites and increases lipid peroxidation in the hypothalamus of WT male mice. **A.** Metabolomic analysis of the hypothalamus showing vitamins and related molecules, amino acids, neurotransmitters and intermediates, nucleosides and nucleotides, bioenergetics substrates and intermediates of metabolic pathways (WT VEH: n = 6; WT OLA: n = 6; PTP1B–KO VEH: n = 6; PTP1B–KO OLA: n = 6, groups were compared using *Student's t-test*). **B.** Lipidomic analysis of the hypothalamus from mice receiving OLA via i.p. (WT VEH: n = 6; WT OLA: n = 6; PTP1B–KO VEH: n = 6; PTP1B–KO OLA: n = 6, groups were compared using *Student's t-test*). **C.** Representative images of hypothalamic sections analyzed by immunohistochemistry against neuroketals and 3-nitrotyrosine in WT and PTP1B–KO male mice i.p. injected with OLA or VEH (20x, scale bars-100 μm) (WT VEH: n = 3; WT OLA: n = 3; PTP1B–KO VEH: n = 3; PTP1B–KO OLA: n = 3). **D.** Representative LDI-MS imaging (one sample *per* group) of peroxidized lipid species corresponding to *(left to right)* **1.** PA (22:2; O), $C_{25}H_{45}O_9P$, $[M+H–H2O]^+$; **2.** PA (21:1; O2), $C_{24}H_{45}O_{10}PNa$, $[M+Na]^+$; **3.** PA (27:2; O), $C_{30}H_{55}O_9PNa$, $[M+Na]^+$; **4.** PE (24:2; O3); $C_{29}H_{54}NO_{11}P$, $[M+H]^+$; **5.** PA (27:2; O), $C_{30}H_{55}O_9PK$, $[M+K]^+$; **6.** PA (27:2; O), $C_{30}H_{55}O_9PK$, $[M+K]^+$; **7.** PA (27:2; O2), $C_{30}H_{55}O_9PK$, $[M+K]^+$; **8.** PA (27:2; O2), $C_{30}H_{55}O_{10}PK$, $[M+K]^+$; **9.** PC (23:3; O2), $C_{31}H_{56}NO_{10}PNa$, $[M+Na]^+$; **10.** PE (26:3; O2), $C_{31}H_{56}NO_{10}PNa$, $[M+Na]^+$; **11.** PC (25:1; O), $C_{33}H_{64}NO_9PNa$, $[M+Na]^+$; **12.** PE (30:3; O2), $C_{35}H_{64}NO_{10}P$, $[M+H–H2O]^+$; **13.** PC (25:3; O2), $C_{33}H_{60}NO_{10}PNa$, $[M+Na]^+$; **14.** PE (28:3; O2), $C_{33}H_{60}NO_{10}PNa$, $[M+Na]^+$; **15.** PC (25:3; O3), $C_{33}H_{60}NO_{10}PNa$, $[M+Na]^+$; **16.** PS (27:2; O), $C_{33}H_{60}NO_{11}PNa$, $[M+Na]^+$; **17.** PC (25:1; O2), $C_{33}H_{64}NO_{10}PK$, $[M+K]^+$; **18.** PC (25:3; O3), $C_{33}H_{60}NO_{11}PK$, $[M+K]^+$; **19.** PS (27:2; O), $C_{33}H_{60}NO_{11}PK$, $[M+K]^+$; **20.** PE (30:3; O3), $C_{35}H_{64}NO_{11}PNa$, $[M+Na]^+$; **21.** PG (30:3; O2), $C_{36}H_{65}O_{12}PNa$, $[M+Na]^+$; **22.** PG (30:3; O2), $C_{36}H_{65}O_{12}PK$, $[M+K]^+$ (more information in Supplementary Table 4). Intensity of each ion (arbitrary units) is color-coded (WT VEH: n = 3; WT OLA: n = 3; PTP1B–KO VEH: n = 3; PTP1B–KO OLA: n = 3). **E.** Representative confocal images of MitoTracker Red CM-H_2Xros staining in GT1-7 hypothalamic neurons stimulated with OLA (12.5 μM) during a short time-period (4 min) with or without pre-treatment with a selective PTP1B inhibitor (iPTP1B, 20 μM, 2 h) and quantification (DMSO: n = 16; OLA: n = 15; iPTP1B: DMSO: n = 8; OLA: n = 7 independent experiments). Each point/bar corresponds to mean ± SEM; comparisons between groups: *p < 0.05; **p < 0.01; ***p < 0.001. (For interpretation of the references to color in this figure legend, the reader is referred to the Web version of this article.)

immunohistochemistry images in Fig. 5C (and Supplementary Figs. 3A and 3B), WT mice under OLA i.p. treatment presented higher levels of neuroketal adducts and 3-nitrotyrosine residues compared to the VEHgroup, supporting an increase in lipid peroxidation and protein nitration, as reported in other contexts [92]. As expected, PTP1B-deficient mice did not show an increase in neuroketals and 3-nitrotyrosine in the hypothalamus, even though higher basal levels compared to those of WT mice were found. A step further, LDI-MS imaging analysis specific for oxidized lipid species evidenced that the drop of antioxidant metabolites in the hypothalamus of WT male mice treated with OLA via i.p. correlated with a significant increase in the peroxidation of glycerophospholipid species (Fig. 5D, Supplementary Table 4). Even though PTP1B-deficient mice receiving OLA i.p. treatment presented a milder increase in the same oxidized glycerophospholipids, contrarily to their WT counterparts, those mice presented also a decrease in other peroxidized species (Supplementary Table 4), suggesting a protective effect against OLA-induced hypothalamic oxidative stress. It is noteworthy to mention that in mice fed an OLA-supplemented diet no significant changes were found in the broad metabolomics analysis of the hypothalamus (Supplementary Figs. 4A and 4B), an effect likely related to lower levels of OLA reaching this brain region upon oral administration [32].

Next, we conducted *in vitro* experiments to test the ability of OLA to induce oxidative stress in hypothalamic neurons. GT1-7 hypothalamic neurons were treated with 12.5 μM OLA during a short time-period (4 min) and MitoTracker Red CM-H_2Xros staining was analyzed by confocal microscopy. As shown in Fig. 5E, OLA induced oxidative stress and, importantly, this effect was absent in cells pre-treated with a selective PTP1B inhibitor for 2 h. Overall, these results support the ability of OLA to mediate hypothalamic oxidative stress which can be prevented by inhibition of PTP1B.

3.4. Effects of OLA i.p. administration in astrocyte and microglia activation in the hypothalamus: protective effect of PTP1B inhibition

Inflammation is often concomitant to oxidative stress in both CNS and periphery [93–96]. In this regard, increased inflammatory features were visualized by NMR imaging in the brain of WT mice after 8 weeks of OLA i.p. treatment (Fig. 6A) or a single OLA intrahypothalamic injection (Fig. 6B and Supplementary Fig. 5A). However, PTP1B–KO mice did not manifest brain inflammation. These results were supported by immunofluorescence analysis of the astrocyte marker glial fibrillary acidic protein (GFAP) in the hypothalamus where a statistically significant increase of $GFAP^+$ cells was found in WT mice receiving OLA via i.p. In addition, immunostaining with the microglial marker Ionized calcium-binding adapter molecule 1 (Iba1) evidenced a higher presence of microglial cells with activated shape exclusively in OLA-treated WT mice compared to their VEH-treated controls (Fig. 6C). Regarding PTP1B–KO mice, as occurred in the liver [35], elevations in inflammatory markers were observed under basal conditions (VEH-treated), without changes associated to OLA administration. Importantly, these hallmarks of oxidative stress and inflammation found in the hypothalamus of WT mice receiving a chronic i.p. treatment with OLA did not result in cell death in this brain region as revealed by absence of TUNEL immunofluorescence signals (Supplementary Fig. 5B). The results in PTP1B–KO mice were reinforced by *in vitro* data in microglia and astrocyte immortalized cell lines where the inhibition of PTP1B with a selective inhibitor (20 μM, 2 h) before OLA treatment prevented IκBα degradation (Fig. 6D). Contrarily to Suh et al. that showed an increase of hypothalamic *Ptpn1* (encoding PTP1B) mRNA levels in female mice orally treated with OLA at 5 mg/kg/day for 5 days, no changes in *Ptpn1* mRNA levels were observed in the hypothalamus of male mice 48 h after an intrahypothalamic OLA injection (Supplementary Fig. 5C).

3.5. JNK1/2 deletion in the hypothalamus prevented hypothalamic inflammation, but not oxidative stress, in mice treated with OLA via i.p.

Next, we attempted to decipher whether activation of JNK1/2 in the hypothalamus links oxidative stress and inflammation in this brain region with FAS upregulation in the liver in mice treated with OLA via i.p. To achieve this, readouts of these two phenomena were analyzed in mice with hypothalamic JNK1/2 deletion that, as shown in Fig. 4B, were protected against OLA-induced elevation of hepatic FAS. Of note, in those mice receiving OLA via i.p. we did not observed changes in neuroketal aggregates, 3-nitrotyrosine residues or oxidized glycerophospholipids in the hypothalamus (Fig. 7A and B and Supplementary Figs. 6A and 6B). These *in vivo* data were supported by pharmacological inhibition of JNK with SP600125 (20 μM) added to GT1-7 hypothalamic neurons 2 h before OLA. As shown in Fig. 6C, SP600125 did not prevent OLA-induced increase in MitoTracker Red CM-H_2Xros staining. However, pre-treatment with NAC (10 mM, 2 h) markedly reduced OLA-induced oxidative stress and also prevented JNK phosphorylation in this cell line (Fig. 7C and D). Altogether, these results point that OLA induces oxidative stress in the hypothalamus in a JNK-independent manner.

Conversely, deletion of JNK1 in the hypothalamus of global JNK2-deficient mice attenuated the effect of OLA in elevating $GFAP^+$ and $Iba1^+$ cells compared to their respective OLA-treated AAV-GFP controls (Fig. 7E). These *in vivo* results were supported by *in vitro* data in microglia and astrocyte cell lines pre-treated with SP600125 prior to OLA which prevented IκBα degradation (Figs. 6E and 7F). These results, together with the absence of JNK1 phosphorylation and inflammation in the hypothalamus of PTP1B–KO mice, point to the requirement of JNK1 activation for the observed neuroinflammation in male mice receiving

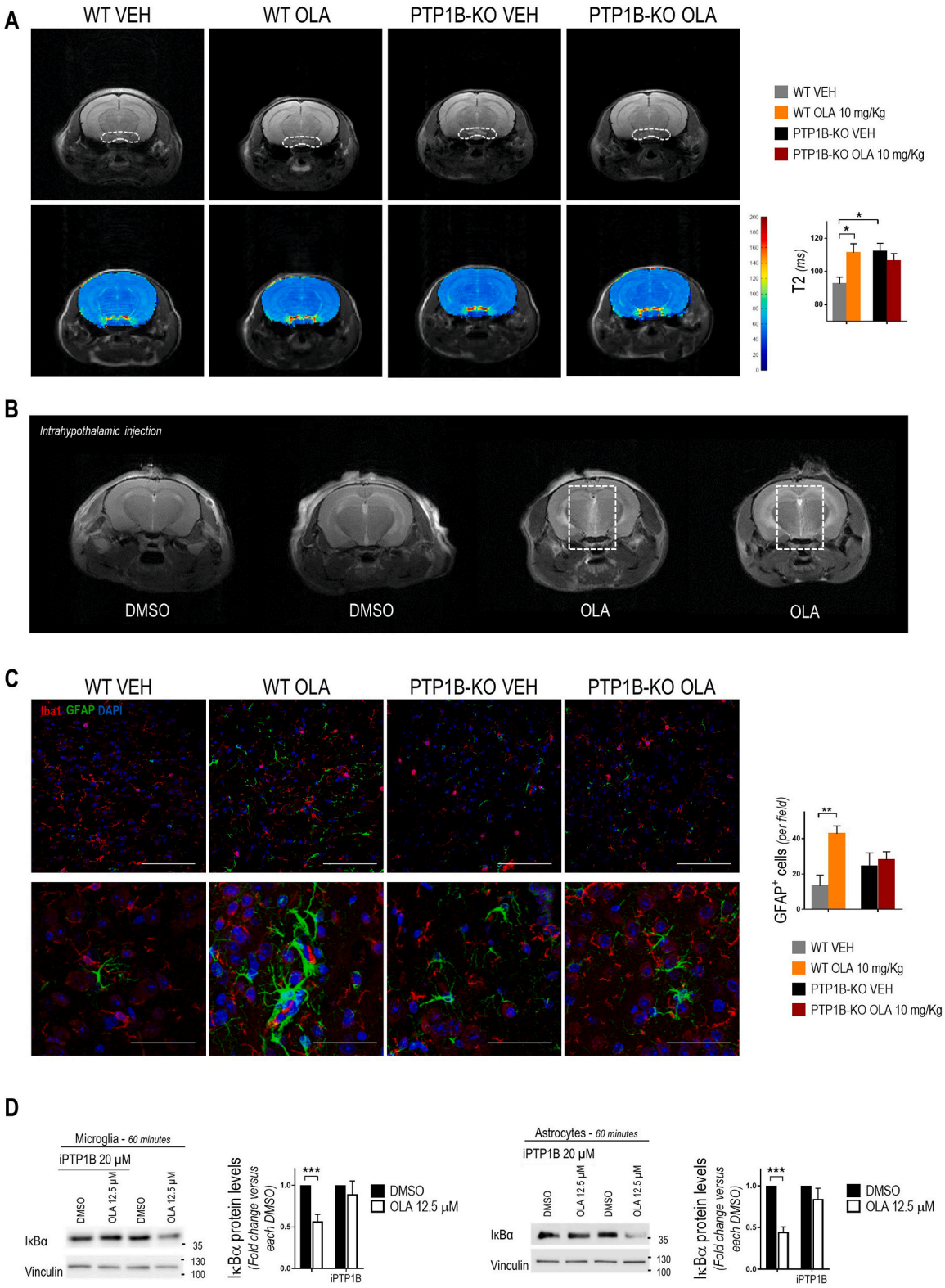

Fig. 6. Effects of OLA i.p. administration in astrocyte and microglia activation in the hypothalamus: protective effect of PTP1B inhibition. **A.** T2 maps of the brain from WT and PTP1B–KO mice treated with OLA via i.p. (WT VEH: n = 5; WT OLA: n = 4; PTP1B–KO VEH: n = 4; PTP1B–KO OLA: n = 4). **B.** NMR images of the brain from mice receiving an intrahypothalamic OLA injection at 48 h post-injection. Inflamed area is indicated by a white square (WT VEH: n = 5; WT OLA: n = 5). **C.** Representative confocal images of Iba1 and GFAP immunofluorescence (20x (*upper panel*), scale bars-100 μm and 63x (*lower panel*), scale bars-50 μm) of OLA-treated mice via i.p. (WT VEH: n = 4; WT OLA: n = 5; PTP1B–KO VEH: n = 3; PTP1B–KO OLA: n = 3; *left panels*) and quantification of $GFAP^+$ cells (WT VEH: n = 4; WT OLA: n = 5; PTP1B–KO VEH: n = 3; PTP1B–KO OLA: n = 3, *right panel*). **D.** Representative Western blot images of IκBα in microglia and astrocytes pre-treated with a selective PTP1B inhibitor (iPTP1B, 20 μM, 2 h) prior to OLA addition (12.5 μM, 30 min) and their respective densitometric quantifications normalized for Vinculin levels (Microglia: DMSO: n = 9; OLA: n = 9; iPTP1B: DMSO: n = 6; OLA: n = 6; Astrocytes: DMSO: n = 11; OLA: n = 11; iPTP1B: DMSO: n = 6; OLA: n = 6 independent experiments). Each point/bar corresponds to mean ± SEM; comparisons between groups: *$p < 0.05$; **$p < 0.01$; ***$p < 0.001$.

OLA treatment via i.p. However, we cannot exclude a synergistic effect of the activation of immune cell populations by OLA and the cell autonomous effect of this SGA in hypothalamic neurons, which likely boosts oxidative stress.

4. Discussion

Several preclinical studies have been conducted to investigate the molecular basis of the metabolic side-effects associated to the treatment with SGAs [8,9]. Among these drugs, OLA has been the focus of many of

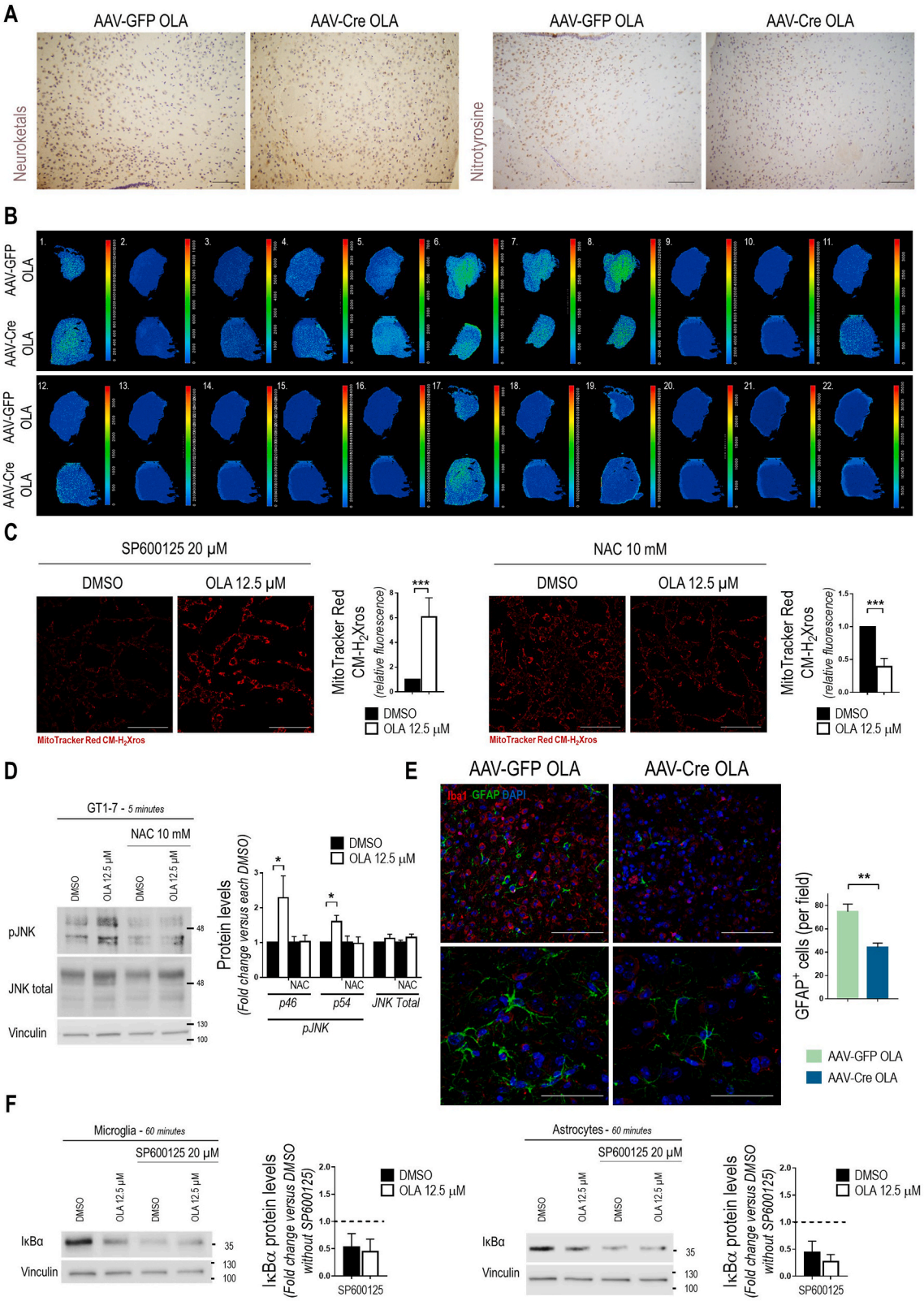

(caption on next page)

Fig. 7. JNK1/2 deletion in the hypothalamus of mice treated with OLA via i.p. prevented hypothalamic inflammation, but not oxidative stress. **A.** Representative images of neuroketals and 3-nitrotyrosine immunohistochemistry of hypothalamic sections of C57BL/6J JNK2-KO/JNK1$^{flox\text{-}flox}$ mice injected AAV-GFP or AAV-Cre in the hypothalamus prior to the treatment with OLA via i.p. (20x, scale bars-100 μm) (AAV-GFP OLA: n = 5; AAV-Cre OLA: n = 5, groups were compared using *Student's t-test*). **B.** Representative LDI-MS imaging (one sample *per* group) of peroxidized lipid species corresponding to *(left to right)* **1.** PA (22:2; O), $C_{25}H_{45}O_9P$, [M+H–H2O]$^+$; **2.** PA (21:1; O2), $C_{24}H_{45}O_{10}PNa$, [M+Na]$^+$; **3.** PA (27:2; O), $C_{30}H_{55}O_9PNa$, [M+Na]$^+$; **4.** PE (24:2; O3); $C_{29}H_{54}NO_{11}P$, [M+H]$^+$; **5.** PA (27:2; O), $C_{30}H_{55}O_9PK$, [M+K]$^+$; **6.** PA (27:2; O), $C_{30}H_{55}O_9PK$, [M+K]$^+$; **7.** PA (27:2; O2), $C_{30}H_{55}O_9PK$, [M+K]$^+$; **8.** PA (27:2; O2), $C_{30}H_{55}O_{10}PK$, [M+K]$^+$; **9.** PC (23:3; O2), $C_{31}H_{56}NO_{10}PNa$, [M+Na]$^+$; **10.** PE (26:3; O2), $C_{31}H_{56}NO_{10}PNa$, [M+Na]$^+$; **11.** PC (25:1; O), $C_{33}H_{64}NO_9PNa$, [M+Na]$^+$; **12.** PE (30:3; O2), $C_{35}H_{64}NO_{10}P$, [M+H–H2O]$^+$; **13.** PC (25:3; O2), $C_{33}H_{60}NO_{10}PNa$, [M+Na]$^+$; **14.** PE (28:3; O2), $C_{33}H_{60}NO_{10}PNa$, [M+Na]$^+$; **15.** PC (25:3; O3), $C_{33}H_{60}NO_{10}PNa$, [M+Na]$^+$; **16.** PS (27:2; O), $C_{33}H_{60}NO_{11}PNa$, [M+Na]$^+$; **17.** PC (25:1; O2), $C_{33}H_{64}NO_{10}PK$, [M+K]$^+$; **18.** PC (25:3; O3), $C_{33}H_{60}NO_{11}PK$, [M+K]$^+$; **19.** PS (27:2; O), $C_{33}H_{60}NO_{11}PK$, [M+K]$^+$; **20.** PE (30:3; O3), $C_{35}H_{64}NO_{11}PNa$, [M+Na]$^+$; **21.** PG (30:3; O2), $C_{36}H_{65}O_{12}PNa$, [M+Na]$^+$; **22.** PG (30:3; O2), $C_{36}H_{65}O_{12}PK$ [M+K]$^+$ (more information in Supplementary Table 4).), in hypothalamic sections of JNK2-KO/JNK1$^{flox\text{-}flox}$ mice injected AAV-GFP and AAV-Cre in the hypothalamus *prior* to the treatment with OLA via i.p. Intensity of each ion (arbitrary units) is color-coded (AAV-GFP OLA: n = 3; AAV-Cre OLA: n = 3). **C.** Representative confocal images from MitoTracker Red CM-H_2Xros staining of GT1-7 hypothalamic neurons pre-treated with SP600125 (20 μM, 2 h) or NAC (10 mM, 2 h) prior to OLA (12.5 μM) stimulation during a short time-period (4 min) and quantification (SP600125: DMSO: n = 8; OLA: n = 8; NAC: DMSO: n = 7; OLA: n = 7). **D.** Representative Western blot images of phosphorylated and total JNK in GT1-7 hypothalamic neurons cell line pre-treated with NAC (10 mM, 2 h) prior to OLA addition (12.5 μM, 5 min). Densitometric quantification of phospho-JNK and total JNK normalized for total JNK and Vinculin protein levels, respectively (DMSO: n = 5; OLA: n = 5; NAC: DMSO: n = 5; OLA: n = 5 independent experiments). **E.** Representative confocal images of Iba1 and GFAP immunofluorescence (20x, scale bars-100 μm and 63x, scale bars-50 μm) in hypothalamic sections of JNK2-KO/JNK1$^{flox\text{-}flox}$ mice injected AAV-GFP and AAV-Cre in the hypothalamus prior to the treatment with OLA via i.p. (AAV-GFP OLA: n = 5; AAV-Cre OLA: n = 4) and quantification of GFAP$^+$ cells (*right panels,* AAV-GFP OLA: n = 5; AAV-Cre OLA: n = 4, groups were compared using *Student's t-test*). **F.** Representative Western blot images of IκBα in microglia (*left panels,* n = 6 independent experiments, groups were compared using *Student's t-test*) and astrocytes (*right panels,* n = 6 independent experiments, groups were compared using *Student's t-test*) pre-treated with SP600125 (20 μM, 2 h) prior to OLA (12.5 μM, 60 min) stimulation and their respective densitometric quantifications normalized for Vinculin levels. Results are expressed in fold of change *versus* DMSO without SP600125 condition. Each point/bar corresponds to mean ± SEM; comparisons between groups: *p < 0.05; **p < 0.01; ***p < 0.001. (For interpretation of the references to color in this figure legend, the reader is referred to the Web version of this article.)

them due to its wide use in clinical practice and the high obesogenic profile found in patients under treatment with this SGA [97,98]. Herein, we report differences in intrahepatic lipid accumulation by administering OLA orally (supplemented in the diet) or via i.p. injection using doses previously reported by our group and others [32,36–48,99]. Moreover, we have shed light into new molecular insights associated with the central-peripheral crosstalk in response to the treatment with OLA via i.p. that, as we recently reported, prevented weight gain in male mice. Specifically, we found: i) the inhibition of PTP1B as an effective approach in preventing intrahepatic lipid accumulation associated to the oral treatment with OLA in male mice; ii) the molecular mechanism by which i.p. injections of OLA prevent intrahepatic lipid accumulation despite of the upregulation of FAS levels through a JNK1-driven hypothalamus-liver crosstalk; iii) the protective effect of PTP1B inhibition against hypothalamic oxidative stress and inflammation during chronic OLA i.p. treatment in which the levels of this SGA reaching the hypothalamus are higher compared to the oral administration.

In our recent study we demonstrated that male mice receiving OLA via i.p. showed body weight loss, an effect associated with the activation of a hypothalamic AMPK-BAT/iWAT UCP-1 axis, in a PTP1B-independent manner, whereas weight gain in mice under oral treatment with OLA was prevented in PTP1B–KO mice due to an increase in EE [32]. Considering this benefit of the OLA i.p. treatment with a potential translational value, herein we aimed to investigate in more detail additional intra- and extra-hypothalamic effects elicited by OLA administration via i.p. since this administration route resulted in significant higher levels of this SGA in plasma and hypothalamus in comparison to those of the oral treatment [32]. As such, we focused the present study in the connection between the hypothalamus and the liver since it has been reported that this axis modulates lipid metabolism in response to T_3 [19] and glucose homeostasis in response to leptin [100,101].

As expected from the changes in body weight, intrahepatic lipid accumulation was found in WT mice upon OLA oral administration and, also not surprisingly [102,103], this effect was absent in PTP1B–KO mice that were protected against weight gain under these experimental settings [32]. In fact, the transcriptomic analysis revealed attenuated changes in gene families associated to hepatic steatosis/NAFLD progression in livers from PTP1B–KO mice fed an OLA-supplemented diet but, on the contrary, these gene families were markedly altered in WT mice (*i.e.* circadian rhythm [104,105], PPAR signaling pathway [106,107], biosynthesis of unsaturated FAs [108,109], glycosaminoglycan biosynthesis [110,111], glycosphingolipid biosynthesis [112,113], terpenoid backbone biosynthesis and steroid biosynthesis [114,115]). These data highlight the protection of PTP1B deficiency against a broad spectrum of obesogenic inducers. Of interest, in WT mice treated with OLA supplemented in the diet, the hepatic levels of FAS, the rate limiting enzyme for *the novo* lipogenesis and the lipid fluxes related to FA and TG synthesis were similar to those from mice receiving chow diet without OLA, suggesting that the intrahepatic lipid accumulation is likely a consequence of the hyperphagia [32] and adiposity [116] induced by the treatment as we recently reported. Additionally, we cannot rule out an impact of the oral chronic treatment with OLA in FA catabolism that might also contribute to intrahepatic TG accumulation.

Surprisingly, we found that FAS was upregulated in the livers from WT mice treated with OLA via i.p., even though those mice did not present hepatic steatosis. This effect is likely due to OLA-induced transcriptional downregulation of *Insig2* which, in turn, increases *Srebf1* expression, as reported in adipose-derived stem cells [117]. Notably, this lipogenic program was not activated in PTP1B–KO mice. Since *de novo* lipogenesis is an anabolic process highly dependent on ATP availability, we measured hepatic ATP content and found that it was depleted in the liver of WT mice after OLA exposure. This ATP deficit concurred with an increase in the phosphorylation of AMPK, a sensor of low energy status, and its target enzyme ACC [118] that leads to their activation and inhibition, respectively, being the latter the first step of β-oxidation. Altogether, these findings suggest that the intrahepatic energy imbalance resulting from OLA i.p. administration might be counteracted by the activation of FA catabolism, thereby avoiding lipid accumulation. Normally, lipogenesis and β-oxidation are opposite regulated in the liver by fasting and feeding; however, in male mice treated with OLA via i.p., hepatic *Insig2/Srebf1/Fasn* expression is also controlled by extrahepatic signals in a nutritional-independent manner and sensed by AMPK/ACC likely due to the reduction in ATP by its utilization in fueling this lipogenic anabolic flux. This molecular rewiring results in a futile cycle where lipids are synthesized but, at the same time, metabolized, probably by β-oxidation, for ATP replenishment. The involvement of extrahepatic signals in the effects of the i.p. OLA treatment was supported by the absence of modulation of FAS/-phospho-ACC by the treatment of primary hepatocytes with the drug *ex vivo*. In this regard, our results in primary hepatocytes differ from those of Zhu and co-workers that found elevations in FAS in hepatic cell lines treated with a higher OLA concentration (100 μM) [17]. A step further, an elevation of FAS protein levels was found in the liver of mice

receiving an OLA intrahypothalamic injection, evidencing signals emerging from the hypothalamus as drivers of the increase in hepatic FAS expression by OLA. Notably, our results differ from those of Martinez-Sanchez et al. [19] that reported hypothalamic-mediated upregulation of hepatic FAS by T_3 concomitantly with decreased AMPK/ACC phosphorylation that resulted in TG synthesis. Since we did not find changes in AMPK/ACC phosphorylation in the liver in the time-frame of 30 min-48 h post-OLA central administration, we hypothesized that OLA i.p. treatment also results in the upregulation of hepatic FAS expression via central signals but, in this case, AMPK/ACC modulation by ATP depletion is likely secondary to *de novo* lipogenesis and the final outcome is the absence of intrahepatic lipid accumulation. Of note, the absence of intrahepatic lipid accumulation in male mice receiving OLA (10 mg/kg/day) via i.p. was corroborated by the work of Zhu et *al.* in females on a chow diet upon the same experimental settings [119].

To understand the molecular basis behind the elevation in FAS protein content in the liver induced by OLA i.p. administration and, considering previous studies that point the activation of JNK1 in the hypothalamus as modulator of hepatic *de novo* lipogenesis [19], we explored the hypothalamic JNK1-liver axis in WT and PTP1B–KO mice. Our results showed increased JNK phosphorylation in the hypothalamus of WT male mice receiving OLA via i.p. and, interestingly, under similar conditions PTP1B-deficient mice did not show hypothalamic JNK activation besides similar levels of this SGA found in this brain region in both genotypes. As stated above, JNK activation was absent in mice receiving oral treatment and, importantly, in those mice significant lower levels of OLA were found in plasma and hypothalamus compared to the i.p. administration [32]. Thus, as occurred in the activation of the hypothalamic AMPK-adipose tissue UCP-1 axis [32], it seems that a threshold of OLA needs to be overcomed to activate the connection between the hypothalamus and the liver. This was supported by the absence of hypothalamic JNK activation in mice receiving OLA at 5 mg/kg/day via i.p. that, as reported in our previous study [32], resulted in a peak of hypothalamic OLA levels comparable to the oral treatment. It is noteworthy to highlight that the peak of OLA levels in plasma reached 200 ng/ml only in the i.p. treatment at 10 mg/kg and gradually decreased reaching levels below 100 ng/ml at 8 h post-injection [32]. By contrast, OLA plasma levels in the oral treatment by gavage reached a lower peak (~80 ng/ml). These data are in accordance with the guidelines for therapeutic drug monitoring in psychiatry, since the plasma concentration of OLA is described to range within 20–80 ng/ml at 12–15 h after dosing in patients with schizophrenia [120–124].

A step further, our results herein demonstrate that the upregulation of hepatic FAS found in mice treated with OLA via i.p. relays on hypothalamic JNK1 activation since its deletion abolishes this effect in the liver. Increased phospho-JNK1 was also found in GT1-7 hypothalamic neurons directly stimulated with OLA, supporting a cell autonomous effect that, as abovementioned, was not found in primary hepatocytes. Additionally, our results in vagotomized mice show that JNK1-mediated hypothalamic signals upregulate hepatic FAS through the vagus nerve, as reported for central T_3 administration [19]. The ability of OLA at 10 mg/kg administered via i.p. to modulate hepatic lipogenesis is supported by Ferno and coworkers [125] showing that an intramuscular injection of OLA at doses ranging from 150 to 250 mg/kg increased *Srebf1* and *Fasn* expression in the liver of male rats in a dose-dependent manner, evidencing in both studies that a threshold of OLA is needed to activate lipogenic gene expression in the liver which herein we found to be controlled by hypothalamic JNK1-mediated signals. Moreover, as previously reported by the same group, female rats receiving a single i.p. injection of OLA presented a rapid and robust elevation of serum free FA and glucose levels followed by hepatic lipid accumulation [126] even though in a more recent study also conducted in female rats, but receiving a long-acting OLA formulation via intramuscular injection [127], they showed up-regulated hepatic *Srebf1* and *Fasn* levels in the liver without TG accumulation, in agreement with our results. Taking all these studies into account, under our experimental settings the peak of OLA reached in the hypothalamus when the dose of 10 mg/kg is administered via i.p. is likely required to activate the hypothalamic JNK1-hepatic FAS axis and, as previously reported [32], the hypothalamic AMPK-adipose tissue UCP1 axis that prevented hepatic steatosis and weight gain, respectively. Of interest, our results support that these two axes controlled by OLA and emerging from the hypothalamus are independent since the modulation of hypothalamic JNK1 does not alter the outcomes of the hypothalamic AMPK-adipose tissue UCP1 axis and *vice versa*. Furthermore, these results were supported by data from PTP1B-deficient mice that preserved OLA-mediated hypothalamic AMPK-adipose tissue thermogenesis and weight loss [32] whereas those mice did not present hypothalamic JNK activation.

It is noteworthy to highlight that our results herein show for the first time that the hypothalamic JNK activation in OLA-treated WT male mice via i.p. correlated with a marked reduction in antioxidant mediators in this brain region [74–83] which, in turn, increases protein nitration and lipid peroxidation, pointing to an increase in ROS levels and augmented oxidative stress in the hypothalamus during chronic OLA treatment by this administration route. These results *in vivo* were supported by the increase in MitoTracker Red CM-H_2Xros staining observed in GT1-7 hypothalamic neurons treated directly with OLA. In this line, the same effect was found in different neuron-derived cell lines including mHypoA-59 neurons treated with a higher concentration of OLA (100 μM) [24] or SH-SY5Y neurons. In the latter, oxidative stress was concomitant with mitochondrial depolarization and damage and increased autophagy [128]. Conversely, other studies revealed antioxidant effects of OLA in neurons. For example, OLA treatment of primary cultured rat cerebral cortical cells resulted in elevation of glutathione S-transferase protein levels and activity [107]. Nevertheless, as expected, our results show that NAC prevented OLA-induced oxidative stress and JNK phosphorylation in GT1-7 hypothalamic neurons but, unexpectedly, this beneficial effect was not found upon JNK inhibition with SP600125, suggesting that OLA induces oxidative stress in the hypothalamus regardless of JNK activation. This was corroborated by the *in vivo* data showing OLA-induced oxidative stress in the hypothalamus of mice with specific deletion of JNK1 in this brain region, reinforcing that JNK1 activation might be secondary to the oxidative stress induced by the OLA i.p. treatment. These results are in line with data from Wu and coworkers that, even though in a different context, reported enhanced JNK phosphorylation and kinase activity in mesangial cells from diabetic mice that was reverted by NAC treatment [129]. Moreover, the abovementioned study shows that JNK inhibition did not reduce oxidative stress. On the other hand, although we did not find neither JNK activation nor features of oxidative stress in WT mice fed an OLA-supplemented diet or in mice treated orally by gavage, again probably by the insufficient levels reaching the hypothalamus, the study of Pillai et al. reported that treatment of male rats for 180 days with OLA (10 mg/kg/day) added to drinking water reduced the expression and activity of the antioxidant enzymes manganese-superoxide dismutase, copper-zinc superoxide dismutase and catalase in cytosolic extracts of whole brain [130].

The present study also provides novel findings on the protective effect of PTP1B deficiency against OLA-mediated oxidative stress in the hypothalamus due, at least in part, to an increase in the levels of metabolites with antioxidant properties. Notably, the higher levels of neuroketal adducts and 3-nitrotyrosine found in the hypothalamus of PTP1B–KO mice under basal conditions (VEH-treated) could result from increased mitochondrial activity as we recently demonstrated in hepatic progenitor cells lacking this phosphatase [131]. It is relevant to highlight that PTP1B inhibition has been proposed as a potential therapeutic strategy for neurological disorders, as reviewed [132], due to the neuroprotective actions of several PTP1B inhibitors (*i.e.* sodium orthovanadate [133], *Mucuna pruriens* extract [134]) that reduced oxidative stress. Of interest, other approaches targeting oxidative stress have been shown to be effective in ameliorating schizophrenia-like symptoms in

preclinical models [135,136].

Oxidative stress coexists with inflammation in both physiological and pathological contexts [137]. This concurrence was found herein in the hypothalamus of OLA-treated mice via i.p. that manifested features of low grade neuroinflammation evidenced by GFAP and Iba-1 immunostaining. In agreement with our results, a previous study in adult male rats treated with OLA (10 mg/kg/day) via osmotic pumps for 8 weeks showed increased density of total microglia and increased Iba-1$^+$ cells with amoeboid morphology in several brain regions including the hypothalamus [138]. In another study, single-cell RNA-sequencing of striatal samples from male mice exposed to OLA supplemented in a high fat diet (50 mg/kg diet) highlighted differences in gene expression in pathways related to neuron/synapse development, alternative splicing and mitochondrial function, as well as in family genes associated with microglial activation and inflammation [139]. *In vitro*, our results also showed cell autonomous effects of OLA by direct activation of inflammatory pathways, specifically by increasing JNK phosphorylation and IκBα degradation in both astrocytes and microglial cells. In this regard, OLA activates human astrocytes via Toll-like Receptor 4/NFκB inflammatory pathway [140]. Mechanistically, we found that the hypothalamic hallmarks of neuroinflammation were absent in mice with JNK1 deletion in this brain region despite of the oxidative stress features. These results suggest that targeting JNK activation is more efficient in ameliorating OLA-mediated inflammation rather than in counteracting oxidative stress. Even though more research will be needed to explain this divergence, our results are supported by the study of Wu et al. in mesangial cells in which JNK inhibition reduced MCP-1 production, but not affected oxidative stress [129]. It is also noteworthy to highlight that, although our goal in the present study is to provide more insights in the hypothalamic-mediated peripheral effects of an i.p. *versus* oral OLA treatment in male mice, females are also susceptible to the oxidative and inflammatory side-effects induced by this SGA [141]. In this regard, additional studies are being carried out to unravel sex-specific effects associated to our findings in energy balance and hepatic lipid metabolism in both i.p. and oral treatment with OLA.

In agreement with the protection against OLA-mediated oxidative stress in the hypothalamus of PTP1B–KO mice, those mice were also protected against the low grade neuroinflammation upon the OLA i.p. treatment. These results are in agreement with our previous study in retinal explants in which a PTP1B inhibitor reduced GFAP levels upon treatment with a cocktail of cytokines [142] highlighting the efficacy of inhibiting PTP1B in reducing neuroinflammation. This was also supported by other studies where PTP1B was inhibited or activated in the CNS. For instance, PTP1B overexpression in microglial cells enhanced nitric oxide production and proinflammatory gene expression following LPS exposure, suggesting that this phosphatase boosts the microglial proinflammatory response [143] whereas a selective PTP1B inhibitor markedly attenuated LPS-mediated inflammation which was corroborated *in vivo* in the hippocampus and cortex of mice. Noteworthy, PTP1B-deficient mice presented elevated basal levels of GFAP positive cells, an effect that could be associated with the basal oxidative stress in the hypothalamus discussed above. Nevertheless, even though a recent study by Suh et al. [144] revealed that female mice orally treated with OLA presented microgliosis which paralleled with an increase of hypothalamic *Ptpn1* mRNA levels, no changes in *Ptpn1* expression were found in the hypothalamus of male mice 48 h post-OLA intrahypothalamic injection despite of the presence of inflammatory features in the brain RMN images. This result leads us to hypothesize that PTP1B expression might not be directly modulated by OLA-induced inflammation in male mice receiving this SGA directly in the hypothalamus. Instead, its inhibition generates a protective environment with more antioxidant/anti-inflammatory players likely preventing OLA-related molecular alterations.

The translational value of our studies is supported by the work of Hunt et al. showing that, even after multiple doses, intravenous OLA administration is safe for patients [145]. Importantly, neuroimaging studies have shown progressive changes in the brain of patients with schizophrenia through time despite of the treatment with antipsychotics [146]. Specifically, the oral treatment with OLA caused adverse changes in the brain structure such as an alteration of cortical thickness in a hemisphere-independent manner [147]. Importantly, OLA treatment has been also associated with a more inflammatory profile in some patients by the increase of proinflammatory cytokines (IFN-γ, IL-4 and IL-6) in plasma [148] and, interestingly, ω-3 FA supplementation improved the cognitive function of patients with schizophrenia that presented metabolic syndrome [149]. Furthermore, even though the effect of oral OLA in the oxidative status of patients is controversial, there are evidences of a mild oxidative stress induced by this SGA [150–152] in agreement with our results. On the other hand, patients under SGA treatment have higher risk of developing NAFLD, particularly those receiving OLA orally [14,153]. These reports highlight the relevance of our findings since an injectable formulation of OLA or the inhibition of PTP1B in combination with OLA administered orally prevented liver steatosis as shown herein, as well as weight gain [32]. Furthermore, clinical trials with PTP1B inhibitors such as trodusquemine (i.e., NCT00606112) are currently undergoing and, surprisingly, schizophrenia-like symptoms were alleviated by trodusquemine in mice [154]. All these findings, together with our results, envision targeting PTP1B as a therapeutic strategy to prevent metabolic side-effects in patients receiving OLA orally, as well as to confer protection against central oxidative stress and inflammation likely associated to long-term injectable treatments. It is noteworthy to highlight the absence of neuronal cell death in the hypothalamus of mice receiving OLA i.p. treatment that support mild and not detrimental effects in this brain region.

In conclusion, this study has shed light into the interactome between the hypothalamus and the liver in response to an OLA i.p treatment, pointing this hypothalamic-driven crosstalk as responsible for a futile cycle in hepatic lipid metabolism which avoids steatosis. These results, together with the protection conferred by PTP1B deficiency against hepatic steatosis in the oral treatment and also against hypothalamic JNK activation, oxidative stress and neuroinflammation in the i.p. treatment, strongly suggest that a therapeutic strategy targeting PTP1B might be also beneficial to prevent metabolic comorbidities in patients under OLA treatment in precision medicine.

Funding

This work was funded by grants PID-2021-122766OB-100 (to AMV), PID2019-104399RB-I00 (to GS) and RTI2018-096061-B-I00 (to XCB) funded by MCIN/AEI/10.13039/501100011033 and "ERDF A way of making Europe" by the European Union. We also acknowledge grants H2020 Marie Sklodowska-Curie ITN-TREATMENT (Grant Agreement 721236, European Commission), P2022/BMD-7227 (Comunidad de Madrid, Spain), Fundación Ramón Areces (Spain) and CIBERdem (ISCIII, Spain) to AMV. VF was a recipient of a contract from ITN-TREATMENT and is currently a PhD fellow from the Portuguese Foundation for Science and Technology (2020.08388.BD, FCT, Portugal)/ERDF. CF was awarded with Sara Borrell contract (CD19/00078, ISCIII, Spain). MGA has a postdoctoral contract 2018 BP 00188 funded by AGAUR (Spain), while CB is recipient of a postdoctoral contract from HORIZON-MSCA-2021-PF-01 MASS2 (Proposal number 101067953).

Authors contribution

The study was designed by VF, PR and ÁMV. Mice treatments, data acquisition, analysis and interpretation were performed by VF, PR and ÁMV. Immunohistochemistry and immunofluorescence analysis were performed by VF. Protein expression analysis was performed by VF, PR and ÁMV. Primary hepatocytes were isolated by PR, IMG, RA and VF. Central injections were performed by VF, MG and PLL. Central adenoviral injections and posterior treatment with OLA were done by VF, CF

and GS. Lipids fluxes studies were done by GD and JGJ. RNAseq and bioinformatics analysis were performed by MRR and JCC and posterior analysis were done by VF, PR, AMV and MRR. Metabolomics, lipidomics and LDI-MS imaging were performed by MGA, CB and XCB, and VF, PR, ÁMV and MGA posteriorly analyzed the data. VF, PR and ÁMV wrote the first draft of the manuscript. CF, MGA, MG, MRR, GD, IGM, RA, JGJ, JCC, PLL, XCB and GS critically revised the manuscript for important intellectual content. All authors gave final approval of the manuscript and gave consent to its publication. ÁMV and PR coordinated the study and ÁMV is the guarantor of the work.

Declaration of competing interest

The authors declare no conflict of interest. Also, the authors declare that there are no relationships or activities that might bias, or be perceived to bias, their work.

Data availability

Data will be made available on request.

Acknowledgements

The authors would like to thank all members of AMV's laboratory for the helpful discussion. We also acknowledge F. Abad-Santos and P. Zubiaur (IIS La Princesa, Madrid, Spain) for the analysis of Olanzapine levels in PTP1B-KO mice and M. Belinchón (IIBm, CSIC) for the technical assistance with the confocal microscopy and Á. Montes for the technical support. The graphical abstract was created with http://Biorender.com.

Appendix A. Supplementary data

Supplementary data to this article can be found online at https://doi.org/10.1016/j.redox.2023.102741.

References

[1] K.R. Patel, J. Cherian, K. Gohil, D. Atkinson, Schizophrenia: overview and treatment options, P T 39 (2014) 638–645.
[2] G. Remington, D. Addington, W. Honer, Z. Ismail, T. Raedler, M. Teehan, Guidelines for the pharmacotherapy of schizophrenia in adults, Can. J. Psychiatr. 62 (2017) 604–616.
[3] D. Cohen, R.P. Stolk, D.E. Grobbee, C.C. Gispen-de Wied, Hyperglycemia and diabetes in patients with schizophrenia or schizoaffective disorders, Diabetes Care 29 (2006) 786–791.
[4] D.E. Casey, Dyslipidemia and atypical antipsychotic drugs, J. Clin. Psychiatry 65 (Suppl 18) (2004) 27–35.
[5] I. Kurzthaler, W.W. Fleischhacker, The clinical implications of weight gain in schizophrenia, J. Clin. Psychiatry 62 (Suppl 7) (2001) 32–37.
[6] K.J. Burghardt, B. Seyoum, A. Mallisho, P.R. Burghardt, R.A. Kowluru, Z. Yi, Atypical antipsychotics, insulin resistance and weight; a meta-analysis of healthy volunteer studies, Prog. Neuro-Psychopharmacol. Biol. Psychiatry 83 (2018) 55–63.
[7] S. Leucht, A. Cipriani, L. Spineli, D. Mavridis, D. Orey, F. Richter, M. Samara, C. Barbui, R.R. Engel, J.R. Geddes, W. Kissling, M.P. Stapf, B. Lassig, G. Salanti, J. M. Davis, Comparative efficacy and tolerability of 15 antipsychotic drugs in schizophrenia: a multiple-treatments meta-analysis, Lancet 382 (2013) 951–962.
[8] V. Ferreira, D. Grajales, A.M. Valverde, Adipose tissue as a target for second-generation (atypical) antipsychotics: a molecular view, Biochim. Biophys. Acta Mol. Cell Biol. Lipids 1865 (2020), 158534.
[9] D. Grajales, V. Ferreira, A.M. Valverde, Second-generation antipsychotics and dysregulation of glucose metabolism: beyond weight gain, Cells 8 (2019).
[10] I. Mikolasevic, S. Milic, T. Turk Wensveen, I. Grgic, I. Jakopcic, D. Stimac, F. Wensveen, L. Orlic, Nonalcoholic fatty liver disease - a multisystem disease? World J. Gastroenterol. 22 (2016) 9488–9505.
[11] M. Mouzaki, T. Yodoshi, A.C. Arce-Clachar, K. Bramlage, L. Fei, S.L. Ley, S. A. Xanthakos, Psychotropic medications are associated with increased liver disease severity in pediatric nonalcoholic fatty liver disease, J. Pediatr. Gastroenterol. Nutr. 69 (2019) 339–343.
[12] M. Amir, M. Yu, P. He, S. Srinivasan, Hepatic autonomic nervous system and neurotrophic factors regulate the pathogenesis and progression of non-alcoholic fatty liver disease, Front. Med. 7 (2020) 62.
[13] O. Soto-Angona, G. Anmella, M.J. Valdes-Florido, N. De Uribe-Viloria, A. F. Carvalho, B. Penninx, M. Berk, Non-alcoholic fatty liver disease (NAFLD) as a neglected metabolic companion of psychiatric disorders: common pathways and future approaches, BMC Med. 18 (2020) 261.
[14] H. Xu, X. Zhuang, Atypical antipsychotics-induced metabolic syndrome and nonalcoholic fatty liver disease: a critical review, Neuropsychiatric Dis. Treat. 15 (2019) 2087–2099.
[15] A.P. Delli Bovi, F. Marciano, C. Mandato, M.A. Siano, M. Savoia, P. Vajro, Oxidative stress in non-alcoholic fatty liver disease, An Updated Mini Review, Front Med (Lausanne) 8 (2021), 595371.
[16] H.M. Soliman, H.M. Wagih, S.A. Algaidi, A.H. Hafiz, Histological evaluation of the role of atypical antipsychotic drugs in inducing non-alcoholic fatty liver disease in adult male albino rats (light and electron microscopic study), Folia Biol. 59 (2013) 173–180.
[17] W. Zhu, C. Ding, P. Huang, J. Ran, P. Lian, Y. Tang, W. Dai, X. Huang, Metformin Ameliorates Hepatic Steatosis induced by olanzapine through inhibiting LXRalpha/PCSK9 pathway, Sci. Rep. 12 (2022) 5639.
[18] R. Li, W. Zhu, P. Huang, Y. Yang, F. Luo, W. Dai, L. Shen, W. Pei, X. Huang, Olanzapine leads to nonalcoholic fatty liver disease through the apolipoprotein A5 pathway, Biomed. Pharmacother. 141 (2021), 111803.
[19] N. Martinez-Sanchez, P. Seoane-Collazo, C. Contreras, L. Varela, J. Villarroya, E. Rial-Pensado, X. Buque, I. Aurrekoetxea, T.C. Delgado, R. Vazquez-Martinez, I. Gonzalez-Garcia, J. Roa, A.J. Whittle, B. Gomez-Santos, V. Velagapudi, Y.C. L. Tung, D.A. Morgan, P.J. Voshol, P.B. Martinez de Morentin, T. Lopez-Gonzalez, L. Linares-Pose, F. Gonzalez, K. Chatterjee, T. Sobrino, G. Medina-Gomez, R. J. Davis, N. Casals, M. Oresic, A.P. Coll, A. Vidal-Puig, J. Mittag, M. Tena-Sempere, M.M. Malagon, C. Dieguez, M.L. Martinez-Chantar, P. Aspichueta, K. Rahmouni, R. Nogueiras, G. Sabio, F. Villarroya, M. Lopez, Hypothalamic AMPK-ER stress-JNK1 Axis mediates the central actions of thyroid hormones on energy balance, Cell Metabol. 26 (2017) 212–229 e212.
[20] Z. Zhu, Y. Gu, C. Zeng, M. Yang, H. Yu, H. Chen, B. Zhang, H. Cai, Olanzapine-induced lipid disturbances: a potential mechanism through the gut microbiota-brain axis, Front. Pharmacol. 13 (2022), 897926.
[21] D. Cui, Y. Peng, C. Zhang, Z. Li, Y. Su, Y. Qi, M. Xing, J. Li, G.E. Kim, K.N. Su, J. Xu, M. Wang, W. Ding, M. Piecychna, L. Leng, M. Hirasawa, K. Jiang, L. Young, Y. Xu, D. Qi, R. Bucala, Macrophage migration inhibitory factor mediates metabolic dysfunction induced by atypical antipsychotic therapy, J. Clin. Invest. 128 (2018) 4997–5007.
[22] E. Hatziagelaki, A. Tsiavou, C. Gerasimou, G.D. Vavougios, A. Spathis, E. Laskos, C. Papageorgiou, A. Douzenis, N. Christodoulou, N. Stefanis, D.A. Spandidos, N. Nikolakakis, K. Tsamakis, E. Rizos, Effects of olanzapine on cytokine profile and brain-derived neurotrophic factor in drug-naive subjects with first-episode psychosis, Exp. Ther. Med. 17 (2019) 3071–3076.
[23] P. Heiser, O. Sommer, A.J. Schmidt, H.W. Clement, A. Hoinkes, U.T. Hopt, E. Schulz, J.C. Krieg, E. Dobschutz, Effects of antipsychotics and vitamin C on the formation of reactive oxygen species, J. Psychopharmacol. 24 (2010) 1499–1504.
[24] Z. Boz, M. Hu, Y. Yu, X.F. Huang, N-acetylcysteine prevents olanzapine-induced oxidative stress in mHypoA-59 hypothalamic neurons, Sci. Rep. 10 (2020), 19185.
[25] F.F. Brinholi, C.C. Farias, K.L. Bonifacio, L. Higachi, R. Casagrande, E.G. Moreira, D.S. Barbosa, Clozapine and olanzapine are better antioxidants than haloperidol, quetiapine, risperidone and ziprasidone in in vitro models, Biomed. Pharmacother. 81 (2016) 411–415.
[26] A. Gonzalez-Rodriguez, J.A. Mas Gutierrez, S. Sanz-Gonzalez, M. Ros, D.J. Burks, A.M. Valverde, Inhibition of PTP1B restores IRS1-mediated hepatic insulin signaling in IRS2-deficient mice, Diabetes 59 (2010) 588–599.
[27] A. Gonzalez-Rodriguez, J.A. Mas-Gutierrez, M. Mirasierra, A. Fernandez-Perez, Y. J. Lee, H.J. Ko, J.K. Kim, E. Romanos, J.M. Carrascosa, M. Ros, M. Vallejo, C. M. Rondinone, A.M. Valverde, Essential role of protein tyrosine phosphatase 1B in obesity-induced inflammation and peripheral insulin resistance during aging, Aging Cell 11 (2012) 284–296.
[28] A. Gonzalez-Rodriguez, B. Santamaria, J.A. Mas-Gutierrez, P. Rada, E. Fernandez-Millan, V. Pardo, C. Alvarez, A. Cuadrado, M. Ros, M. Serrano, A.M. Valverde, Resveratrol treatment restores peripheral insulin sensitivity in diabetic mice in a sirt1-independent manner, Mol. Nutr. Food Res. 59 (2015) 1431–1442.
[29] M. Delibegovic, D. Zimmer, C. Kauffman, K. Rak, E.G. Hong, Y.R. Cho, J.K. Kim, B.B. Kahn, B.G. Neel, K.K. Bence, Liver-specific deletion of protein-tyrosine phosphatase 1B (PTP1B) improves metabolic syndrome and attenuates diet-induced endoplasmic reticulum stress, Diabetes 58 (2009) 590–599.
[30] M.A. Mobasher, A. Gonzalez-Rodriguez, B. Santamaria, S. Ramos, M.A. Martin, L. Goya, P. Rada, L. Letzig, L.P. James, A. Cuadrado, J. Martin-Perez, K. J. Simpson, J. Muntane, A.M. Valverde, Protein tyrosine phosphatase 1B modulates GSK3beta/Nrf2 and IGFIR signaling pathways in acetaminophen-induced hepatotoxicity, Cell Death Dis. 4 (2013) e626.
[31] L. Bourebaba, J. Lyczko, M. Alicka, N. Bourebaba, A. Szumny, A.M. Fal, K. Marycz, Inhibition of protein-tyrosine phosphatase PTP1B and LMPTP promotes palmitate/oleate-challenged HepG2 cell survival by reducing lipoapoptosis, improving mitochondrial dynamics and mitigating oxidative and endoplasmic reticulum stress, J. Clin. Med. 9 (2020).
[32] V. Ferreira, C. Folgueira, M. Guillen, P. Zubiaur, M. Navares, A. Sarsenbayeva, P. Lopez-Larrubia, J.W. Eriksson, M.J. Pereira, F. Abad-Santos, G. Sabio, P. Rada, A.M. Valverde, Modulation of hypothalamic AMPK phosphorylation by olanzapine controls energy balance and body weight, Metabolism 137 (2022), 155335.
[33] J.T. Yue, M.A. Abraham, M.P. LaPierre, P.I. Mighiu, P.E. Light, B.M. Filippi, T. K. Lam, A fatty acid-dependent hypothalamic-DVC neurocircuitry that regulates hepatic secretion of triglyceride-rich lipoproteins, Nat. Commun. 6 (2015) 5970.

[34] Y. Nakade, R. Kitano, T. Yamauchi, S. Kimoto, K. Sakamoto, T. Inoue, Y. Kobayashi, T. Ohashi, Y. Sumida, K. Ito, M. Yoneda, Effect of central corticotropin-releasing factor on hepatic lipid metabolism and inflammation-related gene expression in rats, Int. J. Mol. Sci. 22 (2021).

[35] I. Garcia-Ruiz, N. Blanes Ruiz, P. Rada, V. Pardo, L. Ruiz, A. Blas-Garcia, M. P. Valdecantos, M. Grau Sanz, J.A. Solis Herruzo, A.M. Valverde, Protein tyrosine phosphatase 1b deficiency protects against hepatic fibrosis by modulating nadph oxidases, Redox Biol. 26 (2019), 101263.

[36] D. Grajales, P. Vazquez, M. Ruiz-Rosario, E. Tuduri, M. Mirasierra, V. Ferreira, A. B. Hitos, D. Koller, P. Zubiaur, J.C. Cigudosa, F. Abad-Santos, M. Vallejo, I. Quesada, B. Tirosh, G. Leibowitz, A.M. Valverde, The second-generation antipsychotic drug aripiprazole modulates the serotonergic system in pancreatic islets and induces beta cell dysfunction in female mice, Diabetologia 65 (2022) 490–505.

[37] C.M. Ardic, S. Ilgin, M. Baysal, A.B. Karaduman, V. Kilic, G. Aydogan-Kilic, S. Ucarcan, O. Atli-Eklioglu, Olanzapine induced reproductive toxicity in male rats, Sci. Rep. 11 (2021) 4739.

[38] V.L. Albaugh, C.R. Henry, N.T. Bello, A. Hajnal, S.L. Lynch, B. Halle, C.J. Lynch, Hormonal and metabolic effects of olanzapine and clozapine related to body weight in rodents, Obesity 14 (2006) 36–51.

[39] A.P. Morgan, J.J. Crowley, R.J. Nonneman, C.R. Quackenbush, C.N. Miller, A. K. Ryan, M.A. Bogue, S.H. Paredes, S. Yourstone, I.M. Carroll, T.H. Kawula, M. A. Bower, R.B. Sartor, P.F. Sullivan, The antipsychotic olanzapine interacts with the gut microbiome to cause weight gain in mouse, PLoS One 9 (2014), e115225.

[40] Y.E. Savoy, M.A. Ashton, M.W. Miller, F.M. Nedza, D.K. Spracklin, M. H. Hawthorn, H. Rollema, F.F. Matos, E. Hajos-Korcsok, Differential effects of various typical and atypical antipsychotics on plasma glucose and insulin levels in the mouse: evidence for the involvement of sympathetic regulation, Schizophr. Bull. 36 (2010) 410–418.

[41] H.N. Boyda, L. Tse, R.M. Procyshyn, D. Wong, T.K. Wu, C.C. Pang, A.M. Barr, A parametric study of the acute effects of antipsychotic drugs on glucose sensitivity in an animal model, Prog. Neuro-Psychopharmacol. Biol. Psychiatry 34 (2010) 945–954.

[42] H.N. Boyda, A. Ramos-Miguel, R.M. Procyshyn, E. Topfer, N. Lant, H.H. Choy, R. Wong, L. Li, C.C. Pang, W.G. Honer, A.M. Barr, Routine exercise ameliorates the metabolic side-effects of treatment with the atypical antipsychotic drug olanzapine in rats, Int. J. Neuropsychopharmacol. 17 (2014) 77–90.

[43] V. Mondelli, C. Anacker, A.C. Vernon, A. Cattaneo, S. Natesan, M. Modo, P. Dazzan, S. Kapur, C.M. Pariante, Haloperidol and olanzapine mediate metabolic abnormalities through different molecular pathways, Transl. Psychiatry 3 (2013), e208.

[44] A. Calevro, M.C. Cotel, S. Natesan, M. Modo, A.C. Vernon, V. Mondelli, Effects of chronic antipsychotic drug exposure on the expression of Translocator Protein and inflammatory markers in rat adipose tissue, Psychoneuroendocrinology 95 (2018) 28–33.

[45] M.B. Assie, E. Carilla-Durand, L. Bardin, M. Maraval, M. Aliaga, N. Malfetes, M. Barbara, A. Newman-Tancredi, The antipsychotics clozapine and olanzapine increase plasma glucose and corticosterone levels in rats: comparison with aripiprazole, ziprasidone, bifeprunox and F15063, Eur. J. Pharmacol. 592 (2008) 160–166.

[46] L. Waldman, B. Richardson, J. Hamilton, P. Thanos, Chronic oral olanzapine treatment but not haloperidol decreases [(3)H] MK-801 binding in the rat brain Independent of dietary conditions, Neurosci. Lett. 781 (2022), 136657.

[47] A.V. Terry Jr., S.E. Warner, L. Vandenhuerk, A. Pillai, S.P. Mahadik, G. Zhang, M. G. Bartlett, Negative effects of chronic oral chlorpromazine and olanzapine treatment on the performance of tasks designed to assess spatial learning and working memory in rats, Neuroscience 156 (2008) 1005–1016.

[48] A.V. Terry Jr., W.D. Hill, V. Parikh, D.R. Evans, J.L. Waller, S.P. Mahadik, Differential effects of chronic haloperidol and olanzapine exposure on brain cholinergic markers and spatial learning in rats, Psychopharmacology (Berl) 164 (2002) 360–368.

[49] M. Ikegami, H. Ikeda, T. Ohashi, M. Kai, M. Osada, A. Kamei, J. Kamei, Olanzapine-induced hyperglycemia: possible involvement of histaminergic, dopaminergic and adrenergic functions in the central nervous system, Neuroendocrinology 98 (2013) 224–232.

[50] K.B.J. Franklin, G. Paxinos, Paxinos and Franklin's the Mouse Brain in Stereotaxic Coordinates, fourth ed., Academic Press, an imprint of Elsevier, Place Published, 2013.

[51] M. Lopez, L. Varela, M.J. Vazquez, S. Rodriguez-Cuenca, C.R. Gonzalez, V. R. Velagapudi, D.A. Morgan, E. Schoenmakers, K. Agassandian, R. Lage, P. B. Martinez de Morentin, S. Tovar, R. Nogueiras, D. Carling, C. Lelliott, R. Gallego, M. Oresic, K. Chatterjee, A.K. Saha, K. Rahmouni, C. Dieguez, A. Vidal-Puig, Hypothalamic AMPK and fatty acid metabolism mediate thyroid regulation of energy balance, Nat. Med. 16 (2010) 1001–1008.

[52] P.B. Martinez de Morentin, I. Gonzalez-Garcia, L. Martins, R. Lage, D. Fernandez-Mallo, N. Martinez-Sanchez, F. Ruiz-Pino, J. Liu, D.A. Morgan, L. Pinilla, R. Gallego, A.K. Saha, A. Kalsbeek, E. Fliers, P.H. Bisschop, C. Dieguez, R. Nogueiras, K. Rahmouni, M. Tena-Sempere, M. Lopez, Estradiol regulates brown adipose tissue thermogenesis via hypothalamic AMPK, Cell Metabol. 20 (2014) 41–53.

[53] A. Wojnicz, J.A. Ortiz, A.I. Casas, A.E. Freitas, M.G. Lopez, A. Ruiz-Nuno, Data supporting the rat brain sample preparation and validation assays for simultaneous determination of 8 neurotransmitters and their metabolites using liquid chromatography-tandem mass spectrometry, Data Brief 7 (2016) 714–720.

[54] D. Koller, P. Zubiaur, M. Saiz-Rodriguez, F. Abad-Santos, A. Wojnicz, Simultaneous determination of six antipsychotics, two of their metabolites and caffeine in human plasma by LC-MS/MS using a phospholipid-removal microelution-solid phase extraction method for sample preparation, Talanta 198 (2019) 159–168.

[55] M. Imbernon, D. Beiroa, M.J. Vazquez, D.A. Morgan, C. Veyrat-Durebex, B. Porteiro, A. Diaz-Arteaga, A. Senra, S. Busquets, D.A. Velasquez, O. Al-Massadi, L. Varela, M. Gandara, F.J. Lopez-Soriano, R. Gallego, L.M. Seoane, J.M. Argiles, M. Lopez, R.J. Davis, G. Sabio, F. Rohner-Jeanrenaud, K. Rahmouni, C. Dieguez, R. Nogueiras, Central melanin-concentrating hormone influences liver and adipose metabolism via specific hypothalamic nuclei and efferent autonomic/JNK1 pathways, Gastroenterology 144 (2013) 636–649 e636.

[56] C. Folgueira, D. Beiroa, A. Callon, O. Al-Massadi, S. Barja-Fernandez, A. Senra, J. Ferno, M. Lopez, C. Dieguez, F.F. Casanueva, F. Rohner-Jeanrenaud, L. M. Seoane, R. Nogueiras, Uroguanylin action in the brain reduces weight gain in obese mice via different efferent autonomic pathways, Diabetes 65 (2016) 421–432.

[57] J.C.P. Silva, C. Marques, F.O. Martins, I. Viegas, L. Tavares, M.P. Macedo, J. G. Jones, Determining contributions of exogenous glucose and fructose to de novo fatty acid and glycerol synthesis in liver and adipose tissue, Metab. Eng. 56 (2019) 69–76.

[58] R. Benveniste, T.M. Danoff, J. Ilekis, H.R. Craig, Epidermal growth factor receptor numbers in male and female mouse primary hepatocyte cultures, Cell Biochem. Funct. 6 (1988) 231–235.

[59] P.L. Mellon, J.J. Windle, P.C. Goldsmith, C.A. Padula, J.L. Roberts, R.I. Weiner, Immortalization of hypothalamic GnRH neurons by genetically targeted tumorigenesis, Neuron 5 (1990) 1–10.

[60] N.L. Bray, H. Pimentel, P. Melsted, L. Pachter, Near-optimal probabilistic RNA-seq quantification, Nat. Biotechnol. 34 (2016) 525–527.

[61] M.I. Love, W. Huber, S. Anders, Moderated estimation of fold change and dispersion for RNA-seq data with DESeq2, Genome Biol. 15 (2014) 550.

[62] Y. Liao, J. Wang, E.J. Jaehnig, Z. Shi, B. Zhang, WebGestalt, Gene set analysis toolkit with revamped UIs and APIs, Nucleic Acids Res. 47 (2019) W199–W205, 2019.

[63] Y. Qin, W. Jiang, A. Li, M. Gao, H. Liu, Y. Gao, X. Tian, G. Gong, The combination of paraformaldehyde and glutaraldehyde is a potential fixative for mitochondria, Biomolecules (2021) 11.

[64] E.G. Bligh, W.J. Dyer, A rapid method of total lipid extraction and purification, Can. J. Biochem. Physiol. 37 (1959) 911–917.

[65] L. Lofgren, M. Stahlman, G.B. Forsberg, S. Saarinen, R. Nilsson, G.I. Hansson, The BUME method: a novel automated chloroform-free 96-well total lipid extraction method for blood plasma, J. Lipid Res. 53 (2012) 1690–1700.

[66] R. Barrilero, M. Gil, N. Amigo, C.B. Dias, L.G. Wood, M.L. Garg, J. Ribalta, M. Heras, M. Vinaixa, X. Correig, LipSpin: a new bioinformatics tool for quantitative (1)H NMR lipid profiling, Anal. Chem. 90 (2018) 2031–2040.

[67] J. Gomez, J. Brezmes, R. Mallol, M.A. Rodriguez, M. Vinaixa, R.M. Salek, X. Correig, N. Canellas, Dolphin: a tool for automatic targeted metabolite profiling using 1D and 2D (1)H-NMR data, Anal. Bioanal. Chem. 406 (2014) 7967–7976.

[68] D.S. Wishart, A. Guo, E. Oler, F. Wang, A. Anjum, H. Peters, R. Dizon, Z. Sayeeda, S. Tian, B.L. Lee, M. Berjanskii, R. Mah, M. Yamamoto, J. Jovel, C. Torres-Calzada, M. Hiebert-Giesbrecht, V.W. Lui, D. Varshavi, D. Varshavi, D. Allen, D. Arndt, N. Khetarpal, A. Sivakumaran, K. Harford, S. Sanford, K. Yee, X. Cao, Z. Budinski, J. Liigand, L. Zhang, J. Zheng, R. Mandal, N. Karu, M. Dambrova, H. B. Schioth, R. Greiner, V. Gautam, Hmdb 5.0: the human metabolome database for 2022, Nucleic Acids Res. 50 (2022) D622–D631.

[69] P. Rafols, D. Vilalta, S. Torres, R. Calavia, B. Heijs, L.A. McDonnell, J. Brezmes, E. Del Castillo, O. Yanes, N. Ramirez, X. Correig, Assessing the potential of sputtered gold nanolayers in mass spectrometry imaging for metabolomics applications, PLoS One 13 (2018), e0208908.

[70] P. Rafols, E.D. Castillo, O. Yanes, J. Brezmes, X. Correig, Novel automated workflow for spectral alignment and mass calibration in MS imaging using a sputtered Ag nanolayer, Anal. Chim. Acta 1022 (2018) 61–69.

[71] P. Rafols, S. Torres, N. Ramirez, E. Del Castillo, O. Yanes, J. Brezmes, X. Correig, rMSI: an R package for MS imaging data handling and visualization, Bioinformatics 33 (2017) 2427–2428.

[72] P. Rafols, B. Heijs, E. Del Castillo, O. Yanes, L.A. McDonnell, J. Brezmes, I. Perez-Taboada, M. Vallejo, M. Garcia-Altares, X. Correig, rMSIproc: an R package for mass spectrometry imaging data processing, Bioinformatics 36 (2020) 3618–3619.

[73] K. Schmelzer, E. Fahy, S. Subramaniam, E.A. Dennis, The lipid maps initiative in lipidomics, Methods Enzymol. 432 (2007) 171–183.

[74] P. Sestili, C. Martinelli, E. Colombo, E. Barbieri, L. Potenza, S. Sartini, C. Fimognari, Creatine as an antioxidant, Amino Acids 40 (2011) 1385–1396.

[75] N. Grosser, S. Oberle, G. Berndt, K. Erdmann, A. Hemmerle, H. Schroder, Antioxidant action of L-alanine: heme oxygenase-1 and ferritin as possible mediators, Biochem. Biophys. Res. Commun. 314 (2004) 351–355.

[76] L. Weng, L. Li, L. Ji, D. Zhao, Z. Xu, J. Su, B. Li, X. Zhang, Antioxidant profile of 1-monocaffeoyl glycerol in lipophobic/lipophilic media, J. Food Sci. 84 (2019) 2091–2100.

[77] N. Yanai, S. Shiotani, S. Hagiwara, H. Nabetani, M. Nakajima, Antioxidant combination inhibits reactive oxygen species mediated damage, Biosci. Biotechnol. Biochem. 72 (2008) 3100–3106.

[78] Z. Wang, J. Zhang, L. Chen, J. Li, H. Zhang, X. Guo, Glycine suppresses AGE/RAGE signaling pathway and subsequent oxidative stress by restoring Glo1 function in the aorta of diabetic rats and in HUVECs, Oxid. Med. Cell. Longev. (2019), 4628962, 2019.

[79] R.E. Beyer, The role of ascorbate in antioxidant protection of biomembranes: interaction with vitamin E and coenzyme Q, J. Bioenerg. Biomembr. 26 (1994) 349–358.
[80] P. Wu, W.D. Jiang, Y. Liu, G.F. Chen, J. Jiang, S.H. Li, L. Feng, X.Q. Zhou, Effect of choline on antioxidant defenses and gene expressions of Nrf2 signaling molecule in the spleen and head kidney of juvenile Jian carp (Cyprinus carpio var. Jian), Fish Shellfish Immunol. 38 (2014) 374–382.
[81] A.K. Mehta, N. Arora, S.N. Gaur, B.P. Singh, Choline supplementation reduces oxidative stress in mouse model of allergic airway disease, Eur. J. Clin. Invest. 39 (2009) 934–941.
[82] R.S. Harapanhalli, V. Yaghmai, D. Giuliani, R.W. Howell, D.V. Rao, Antioxidant effects of vitamin C in mice following X-irradiation, Res. Commun. Mol. Pathol. Pharmacol. 94 (1996) 271–287.
[83] A. Meister, On the antioxidant effects of ascorbic acid and glutathione, Biochem. Pharmacol. 44 (1992) 1905–1915.
[84] G. Zhang, L. Zhao, J. Zhu, Y. Feng, X. Wu, Anti-inflammatory activities and glycerophospholipids metabolism in KLA-stimulated RAW 264.7 macrophage cells by diarylheptanoids from the rhizomes of Alpinia officinarum, Biomed. Chromatogr. 32 (2018).
[85] P.V. Subbaiah, R.M. Sargis, Sphingomyelin: a natural modulator of membrane homeostasis and inflammation, Med. Hypotheses 57 (2001) 135–138.
[86] G. Eros, G. Varga, R. Varadi, M. Czobel, J. Kaszaki, M. Ghyczy, M. Boros, Anti-inflammatory action of a phosphatidylcholine, phosphatidylethanolamine and N-acylphosphatidylethanolamine-enriched diet in carrageenan-induced pleurisy, Eur. Surg. Res. 42 (2009) 40–48.
[87] A. Gil, Polyunsaturated fatty acids and inflammatory diseases, Biomed. Pharmacother. 56 (2002) 388–396.
[88] I.M. Medeiros-de-Moraes, C.F. Goncalves-de-Albuquerque, A.R.M. Kurz, F.M. J. Oliveira, V.H.P. de Abreu, R.C. Torres, V.F. Carvalho, V. Estato, P.T. Bozza, M. Sperandio, H.C. de Castro-Faria-Neto, A.R. Silva, Omega-9 oleic acid, the main compound of olive oil, mitigates inflammation during experimental sepsis, Oxid. Med. Cell. Longev. (2018), 6053492, 2018.
[89] J.C. Maroon, J.W. Bost, Omega-3 fatty acids (fish oil) as an anti-inflammatory: an alternative to nonsteroidal anti-inflammatory drugs for discogenic pain, Surg. Neurol. 65 (2006) 326–331.
[90] J.K. Innes, P.C. Calder, Omega-6 fatty acids and inflammation, Prostaglandins Leukot. Essent. Fatty Acids 132 (2018) 41–48.
[91] H.W. Yum, H.K. Na, Y.J. Surh, Anti-inflammatory effects of docosahexaenoic acid: implications for its cancer chemopreventive potential, Semin. Cancer Biol. 40–41 (2016) 141–159.
[92] Y. Sidorova, A. Domanskyi, Detecting oxidative stress biomarkers in neurodegenerative disease models and patients, Methods Protoc 3 (2020).
[93] S. Amor, L.A. Peferoen, D.Y. Vogel, M. Breur, P. van der Valk, D. Baker, J.M. van Noort, Inflammation in neurodegenerative diseases–an update, Immunology 142 (2014) 151–166.
[94] H. Solleiro-Villavicencio, S. Rivas-Arancibia, Effect of chronic oxidative stress on neuroinflammatory response mediated by CD4(+)T cells in neurodegenerative diseases, Front. Cell. Neurosci. 12 (2018) 114.
[95] S. Salim, Oxidative stress and the central nervous system, J. Pharmacol. Exp. Therapeut. 360 (2017) 201–205.
[96] K. Reyes-Gordillo, R. Shah, P. Muriel, Oxidative stress and inflammation in hepatic diseases: current and future therapy, Oxid. Med. Cell. Longev. (2017), 3140673, 2017.
[97] M.V. Seeman, Secondary effects of antipsychotics: women at greater risk than men, Schizophr. Bull. 35 (2009) 937–948.
[98] S. Jain, M. Bhargava, S. Gautam, Weight gain with olanzapine: drug, gender or age? Indian J. Psychiatr. 48 (2006) 39–42.
[99] A.V. Terry Jr., D.A. Gearhart, S.P. Mahadik, S. Warsi, L.W. Davis, J.L. Waller, Chronic exposure to typical or atypical antipsychotics in rodents: temporal effects on central alpha7 nicotinic acetylcholine receptors, Neuroscience 136 (2005) 519–529.
[100] B. Thorens, Neuronal regulation of glucagon secretion and gluconeogenesis, J Diabetes Investig 13 (2022) 599–607.
[101] Y. Ito, R. Sun, H. Yagimuma, K. Taki, A. Mizoguchi, T. Kobayashi, M. Sugiyama, T. Onoue, T. Tsunekawa, H. Takagi, D. Hagiwara, S. Iwama, H. Suga, H. Konishi, H. Kiyama, H. Arima, R. Banno, Protein tyrosine phosphatase 1B deficiency improves glucose homeostasis in type 1 diabetes treated with leptin, Diabetes 71 (2022) 1902–1914.
[102] M. Elchebly, P. Payette, E. Michaliszyn, W. Cromlish, S. Collins, A.L. Loy, D. Normandin, A. Cheng, J. Himms-Hagen, C.C. Chan, C. Ramachandran, M. J. Gresser, M.L. Tremblay, B.P. Kennedy, Increased insulin sensitivity and obesity resistance in mice lacking the protein tyrosine phosphatase-1B gene, Science 283 (1999) 1544–1548.
[103] L.D. Klaman, O. Boss, O.D. Peroni, J.K. Kim, J.L. Martino, J.M. Zabolotny, N. Moghal, M. Lubkin, Y.B. Kim, A.H. Sharpe, A. Stricker-Krongrad, G.I. Shulman, B.G. Neel, B.B. Kahn, Increased energy expenditure, decreased adiposity, and tissue-specific insulin sensitivity in protein-tyrosine phosphatase 1B-deficient mice, Mol. Cell Biol. 20 (2000) 5479–5489.
[104] D. Shi, J. Chen, J. Wang, J. Yao, Y. Huang, G. Zhang, Z. Bao, Circadian clock genes in the metabolism of non-alcoholic fatty liver disease, Front. Physiol. 10 (2019) 423.
[105] A.R. Saran, S. Dave, A. Zarrinpar, Circadian rhythms in the pathogenesis and treatment of fatty liver disease, Gastroenterology 158 (2020) 1948–1966, e1941.
[106] J. Pan, W. Zhou, R. Xu, L. Xing, G. Ji, Y. Dang, Natural PPARs agonists for the treatment of nonalcoholic fatty liver disease, Biomed. Pharmacother. 151 (2022), 113127.
[107] K.H. Liss, B.N. Finck, PPARs and nonalcoholic fatty liver disease, Biochimie 136 (2017) 65–74.
[108] J.G. Gormaz, R. Rodrigo, L.A. Videla, M. Beems, Biosynthesis and bioavailability of long-chain polyunsaturated fatty acids in non-alcoholic fatty liver disease, Prog. Lipid Res. 49 (2010) 407–419.
[109] M. Friden, F. Rosqvist, H. Ahlstrom, H.G. Niessen, C. Schultheis, P. Hockings, J. Hulthe, A. Gummesson, A. Wanders, F. Rorsman, U. Riserus, J. Vessby, Hepatic unsaturated fatty acids are linked to lower degree of fibrosis in non-alcoholic fatty liver disease, Front. Med. 8 (2021), 814951.
[110] S. Nadanaka, T. Hashiguchi, H. Kitagawa, Aberrant glycosaminoglycan biosynthesis by tumor suppressor EXTL2 deficiency promotes liver inflammation and tumorigenesis through Toll-like 4 receptor signaling, Faseb. J. 34 (2020) 8385–8401.
[111] A.R. Pessentheiner, G.M. Ducasa, P. Gordts, Proteoglycans in obesity-associated metabolic dysfunction and meta-inflammation, Front. Immunol. 11 (2020) 769.
[112] H. Zhao, M. Przybylska, I.H. Wu, J. Zhang, P. Maniatis, J. Pacheco, P. Piepenhagen, D. Copeland, C. Arbeeny, J.A. Shayman, J.M. Aerts, C. Jiang, S. H. Cheng, N.S. Yew, Inhibiting glycosphingolipid synthesis ameliorates hepatic steatosis in obese mice, Hepatology 50 (2009) 85–93.
[113] P. Sen, O. Govaere, T. Sinioja, A. McGlinchey, D. Geng, V. Ratziu, E. Bugianesi, J. M. Schattenberg, A. Vidal-Puig, M. Allison, S. Cockell, A.K. Daly, T. Hyotylainen, Q.M. Anstee, M. Oresic, Quantitative modeling of human liver reveals dysregulation of glycosphingolipid pathways in nonalcoholic fatty liver disease, iScience 25 (2022), 104949.
[114] H. Yang, M. Arif, M. Yuan, X. Li, K. Shong, H. Turkez, J. Nielsen, M. Uhlen, J. Boren, C. Zhang, A. Mardinoglu, A network-based approach reveals the dysregulated transcriptional regulation in non-alcoholic fatty liver disease, iScience 24 (2021), 103222.
[115] Y. Ma, C. Kan, H. Qiu, Y. Liu, N. Hou, F. Han, J. Shi, X. Sun, Transcriptomic analysis reveals the protective effects of empagliflozin on lipid metabolism in nonalcoholic fatty liver disease, Front. Pharmacol. 12 (2021), 793586.
[116] M. Vranic, F. Ahmed, S. Hetty, A. Sarsenbayeva, V. Ferreira, G. Fanni, A. M. Valverde, J.W. Eriksson, M.J. Pereira, Effects of the second-generation antipsychotic drugs aripiprazole and olanzapine on human adipocyte differentiation, Mol. Cell. Endocrinol. 561 (2023), 111828.
[117] C.C. Chen, L.W. Hsu, K.T. Huang, S. Goto, C.L. Chen, T. Nakano, Overexpression of Insig-2 inhibits atypical antipsychotic-induced adipogenic differentiation and lipid biosynthesis in adipose-derived stem cells, Sci. Rep. 7 (2017), 10901.
[118] B.B. Kahn, T. Alquier, D. Carling, D.G. Hardie, AMP-activated protein kinase: ancient energy gauge provides clues to modern understanding of metabolism, Cell Metabol. 1 (2005) 15–25.
[119] Z. Zhu, T. Cao, H. Chen, B. Zhang, C. Lin, H. Cai, Olanzapine-induced nonalcoholic fatty liver disease: the effects of differential food pattern and the involvement of PGRMC1 signaling, Food Chem. Toxicol. 176 (2023), 113757.
[120] N. Bergemann, A. Frick, P. Parzer, J. Kopitz, Olanzapine plasma concentration, average daily dose, and interaction with co-medication in schizophrenic patients, Pharmacopsychiatry 37 (2004) 63–68.
[121] C.J. Bachmann, M. Haberhausen, M. Heinzel-Gutenbrunner, H. Remschmidt, F. M. Theisen, Large intraindividual variability of olanzapine serum concentrations in adolescent patients, Ther. Drug Monit. 30 (2008) 108–112.
[122] L. Citrome, V.L. Stauffer, L. Chen, B.J. Kinon, D.L. Kurtz, J.G. Jacobson, R. F. Bergstrom, Olanzapine plasma concentrations after treatment with 10, 20, and 40 mg/d in patients with schizophrenia: an analysis of correlations with efficacy, weight gain, and prolactin concentration, J. Clin. Psychopharmacol. 29 (2009) 278–283.
[123] C. Hiemke, P. Baumann, N. Bergemann, A. Conca, O. Dietmaier, K. Egberts, M. Fric, M. Gerlach, C. Greiner, G. Grunder, E. Haen, U. Havemann-Reinecke, E. Jaquenoud Sirot, H. Kirchherr, G. Laux, U.C. Lutz, T. Messer, M.J. Muller, B. Pfuhlmann, B. Rambeck, P. Riederer, B. Schoppek, J. Stingl, M. Uhr, S. Ulrich, R. Waschgler, G. Zernig, AGNP consensus guidelines for therapeutic drug monitoring in psychiatry: update 2011, Pharmacopsychiatry 44 (2011) 195–235.
[124] M.L. Lu, Y.X. Wu, C.H. Chen, P.T. Kuo, Y.H. Chen, C.H. Lin, T.H. Wu, Application of plasma levels of olanzapine and N-Desmethyl-Olanzapine to monitor clinical efficacy in patients with schizophrenia, PLoS One 11 (2016), e0148539.
[125] J. Ferno, K.M. Ersland, I.H. Duus, I. Gonzalez-Garcia, K.O. Fossan, R.K. Berge, V. M. Steen, S. Skrede, Olanzapine depot exposure in male rats: dose-dependent lipogenic effects without concomitant weight gain, Eur. Neuropsychopharmacol 25 (2015) 923–932.
[126] G. Jassim, S. Skrede, M.J. Vazquez, H. Wergedal, A.O. Vik-Mo, N. Lunder, C. Dieguez, A. Vidal-Puig, R.K. Berge, M. Lopez, V.M. Steen, J. Ferno, Acute effects of orexigenic antipsychotic drugs on lipid and carbohydrate metabolism in rat, Psychopharmacology (Berl) 219 (2012) 783–794.
[127] S. Skrede, L. Martins, R.K. Berge, V.M. Steen, M. Lopez, J. Ferno, Olanzapine depot formulation in rat: a step forward in modelling antipsychotic-induced metabolic adverse effects, Int. J. Neuropsychopharmacol. 17 (2014) 91–104.
[128] L. Vucicevic, M. Misirkic-Marjanovic, V. Paunovic, T. Kravic-Stevovic, T. Martinovic, D. Ciric, N. Maric, S. Petricevic, L. Harhaji-Trajkovic, V. Bumbasirevic, V. Trajkovic, Autophagy inhibition uncovers the neurotoxic action of the antipsychotic drug olanzapine, Autophagy 10 (2014) 2362–2378.
[129] J. Wu, C. Mei, H. Vlassara, G.E. Striker, F. Zheng, Oxidative stress-induced JNK activation contributes to proinflammatory phenotype of aging diabetic mesangial cells, Am. J. Physiol. Ren. Physiol. 297 (2009) F1622–F1631.
[130] A. Pillai, V. Parikh, A.V. Terry Jr., S.P. Mahadik, Long-term antipsychotic treatments and crossover studies in rats: differential effects of typical and atypical agents on the expression of antioxidant enzymes and membrane lipid peroxidation in rat brain, J. Psychiatr. Res. 41 (2007) 372–386.

[131] I. Barahona, P. Rada, S. Calero-Perez, R. Grillo-Risco, L. Pereira, M.C. Soler-Vazquez, L.M. LaIglesia, M.J. Moreno-Aliaga, L. Herrero, D. Serra, C. Garcia-Monzon, A. Gonzalez-Rodriguez, J. Balsinde, F. Garcia-Garcia, M.P. Valdecantos, A.M. Valverde, Ptpn1 Deletion Protects Oval Cells against Lipoapoptosis by Favoring Lipid Droplet Formation and Dynamics, Cell Death Differ, 2022.
[132] J. Olloquequi, A. Cano, E. Sanchez-Lopez, M. Carrasco, E. Verdaguer, A. Fortuna, J. Folch, M. Bullo, C. Auladell, A. Camins, M. Ettcheto, Protein tyrosine phosphatase 1B (PTP1B) as a potential therapeutic target for neurological disorders, Biomed. Pharmacother. 155 (2022), 113709.
[133] A. Akhtar, M. Bishnoi, S.P. Sah, Sodium orthovanadate improves learning and memory in intracerebroventricular-streptozotocin rat model of Alzheimer's disease through modulation of brain insulin resistance induced tau pathology, Brain Res. Bull. 164 (2020) 83–97.
[134] S.K. Yadav, J. Prakash, S. Chouhan, S.P. Singh, Mucuna pruriens seed extract reduces oxidative stress in nigrostriatal tissue and improves neurobehavioral activity in paraquat-induced Parkinsonian mouse model, Neurochem. Int. 62 (2013) 1039–1047.
[135] T. Sumiyoshi, Y. Higuchi, T. Uehara, Neural basis for the ability of atypical antipsychotic drugs to improve cognition in schizophrenia, Front. Behav. Neurosci. 7 (2013) 140.
[136] J.Q. Liang, X. Chen, Y. Cheng, Paeoniflorin rescued MK-801-induced schizophrenia-like behaviors in mice via oxidative stress pathway, Front. Nutr. 9 (2022), 870032.
[137] A. Dandekar, R. Mendez, K. Zhang, Cross talk between ER stress, oxidative stress, and inflammation in health and disease, Methods Mol. Biol. 1292 (2015) 205–214.
[138] M.C. Cotel, E.M. Lenartowicz, S. Natesan, M.M. Modo, J.D. Cooper, S.C. Williams, S. Kapur, A.C. Vernon, Microglial activation in the rat brain following chronic antipsychotic treatment at clinically relevant doses, Eur. Neuropsychopharmacol 25 (2015) 2098–2107.
[139] A. Abrantes, P. Giusti-Rodriguez, N. Ancalade, S. Sekle, M.L. Basiri, G.D. Stuber, P.F. Sullivan, R. Hultman, Gene expression changes following chronic antipsychotic exposure in single cells from mouse striatum, Mol. Psychiatr. 27 (2022) 2803–2812.
[140] M. He, K. Qian, Y. Zhang, X.F. Huang, C. Deng, B. Zhang, G. Gao, J. Li, H. Xie, T. Sun, Olanzapine-induced activation of hypothalamic astrocytes and toll-like receptor-4 signaling via endoplasmic reticulum stress were related to olanzapine-induced weight gain, Front. Neurosci. 14 (2020), 589650.
[141] M. He, X.F. Huang, G. Gao, T. Zhou, W. Li, J. Hu, J. Chen, J. Li, T. Sun, Olanzapine-induced endoplasmic reticulum stress and inflammation in the hypothalamus were inhibited by an ER stress inhibitor 4-phenylbutyrate, Psychoneuroendocrinology 104 (2019) 286–299.
[142] A.I. Arroba, A.M. Valverde, Inhibition of protein tyrosine phosphatase 1B improves IGF-I receptor signaling and protects against inflammation-induced gliosis in the retina, Invest. Ophthalmol. Vis. Sci. 56 (2015) 8031–8044.
[143] G.J. Song, M. Jung, J.H. Kim, H. Park, M.H. Rahman, S. Zhang, Z.Y. Zhang, D. H. Park, H. Kook, I.K. Lee, K. Suk, A novel role for protein tyrosine phosphatase 1B as a positive regulator of neuroinflammation, J. Neuroinflammation 13 (2016) 86.
[144] S.B. Suh, N. Lee, J. Kim, S. Kim, S. Jang, J.K. Park, K. Lee, S.Y. Choi, H.J. Kwon, C. H. Lee, Metformin ameliorates olanzapine-induced obesity and glucose intolerance by regulating hypothalamic inflammation and microglial activation in female mice, Front. Pharmacol. 13 (2022), 906717.
[145] N.F. Hunt, K.C. McLaughlin, M.P. Kovacevic, K.E. Lupi, K.M. Dube, Safety of intravenous olanzapine administration at a tertiary academic medical center, Ann. Pharmacother. 55 (2021) 1127–1133.
[146] B.C. Ho, N.C. Andreasen, P. Nopoulos, S. Arndt, V. Magnotta, M. Flaum, Progressive structural brain abnormalities and their relationship to clinical outcome: a longitudinal magnetic resonance imaging study early in schizophrenia, Arch. Gen. Psychiatr. 60 (2003) 585–594.
[147] A.N. Voineskos, B.H. Mulsant, E.W. Dickie, N.H. Neufeld, A.J. Rothschild, E. M. Whyte, B.S. Meyers, G.S. Alexopoulos, M.J. Hoptman, J.P. Lerch, A.J. Flint, Effects of antipsychotic medication on brain structure in patients with major depressive disorder and psychotic features: neuroimaging findings in the context of a randomized placebo-controlled clinical trial, JAMA Psychiatr. 77 (2020) 674–683.
[148] M. Moller, S. Fredholm, M.E. Jensen, G. Wortwein, J.R. Larsen, T. Vilsboll, N. Odum, A. Fink-Jensen, Proinflammatory biomarkers are associated with prediabetes in patients with schizophrenia, CNS Spectr. 27 (2022) 347–354.
[149] W. Tang, Y. Wang, F. Xu, W. Fan, Y. Zhang, K. Fan, W. Wang, Y. Zhang, C. Zhang, Omega-3 fatty acids ameliorate cognitive dysfunction in schizophrenia patients with metabolic syndrome, Brain Behav. Immun. 88 (2020) 529–534.
[150] O.P. Singh, I. Chakraborty, A. Dasgupta, S. Datta, A comparative study of oxidative stress and interrelationship of important antioxidants in haloperidol and olanzapine treated patients suffering from schizophrenia, Indian J. Psychiatr. 50 (2008) 171–176.
[151] A. Dietrich-Muszalska, J. Malinowska, B. Olas, R. Glowacki, E. Bald, B. Wachowicz, J. Rabe-Jablonska, The oxidative stress may be induced by the elevated homocysteine in schizophrenic patients, Neurochem. Res. 37 (2012) 1057–1062.
[152] A. Dietrich-Muszalska, B. Olas, R. Glowacki, E. Bald, Oxidative/nitrative modifications of plasma proteins and thiols from patients with schizophrenia, Neuropsychobiology 59 (2009) 1–7.
[153] M. Gunther, J.A. Dopheide, Antipsychotic safety in liver disease: a narrative review and practical guide for the clinician, J. Acad. Consult Liaison Psychiatry 64 (2022) 73–82.
[154] Z. Qin, L. Zhang, M.A. Zasloff, A.F.R. Stewart, H.H. Chen, Ketamine's schizophrenia-like effects are prevented by targeting PTP1B, Neurobiol. Dis. 155 (2021), 105397.